GEAP-4215

FUEL CYCLE PROGRAM. A BOILING WATER REACTOR RESEARCH AND DEVELOPMENT PROGRAM

Eleventh Quarterly Progress Report, January — March, 1963

Compiled by
C. L. Howard

April 5, 1963

Atomic Power Equipment Department
General Electric Company
San Jose, California

UNITED STATES ATOMIC ENERGY COMMISSION • DIVISION OF TECHNICAL INFORMATION

LEGAL NOTICE

Printed in USA. Price $1.50. Available from the Office of Technical Services, Department of Commerce, Washington 25, D. C.

USAEC Division of Technical Information Extension, Oak Ridge, Tennessee

GEAP-4215
REACTOR TECHNOLOGY

FUEL CYCLE PROGRAM

A BOILING WATER REACTOR RESEARCH AND DEVELOPMENT PROGRAM

ELEVENTH QUARTERLY PROGRESS REPORT

January - March 1963

Compiled by
C. L. Howard

April 5, 1963

U. S. ATOMIC ENERGY COMMISSION
CONTRACT AT(04-3)-189
PROJECT AGREEMENT 11

ATOMIC POWER EQUIPMENT DEPARTMENT

GENERAL ELECTRIC

SAN JOSE, CALIFORNIA

ACKNOWLEDGMENT

The Fuel Cycle Program is sponsored by the AEC and is conducted by the General Electric Company with the following individuals contributing to the program during the quarter:

Project Engineer	C. L. Howard
Project Consultant	S. Levy
Fuel Development	T. J. Pashos
	H. E. Williamson
	C. J. Baroch
	J. P. Hoffman
	F. H. Megerth
	S. Y. Ogawa
	J. A. Whittington
Stability	W. H. Cook
	J. M. Case
	R. J. Colmar
	R. O. Niemi
	J. C. Rawlings
Heat Transfer and Fluid Dynamics	E. Janssen
	J. E. Hench
	C. L. Howard
	J. A. Kervinen
	F. E. Tippets
Experimental Physics	D. L. Fischer
	M. R. Hackney
	C. P. Ruiz
VBWR Core Analysis	J. O. Arterburn
	R. A. Becker
	T. Tillinghast
VBWR Programming	H. D. Ongman
VBWR Operation	J. B. Violette
	E. L. Burley
	VBWR Staff
Vallecitos Radioactive Material Laboratory	R. F. Boyle

TABLE OF CONTENTS

LIST OF TABLES

LIST OF ILLUSTRATIONS

INTRODUCTION

The fuel Cycle Program is an integrated program of investigation in the Vallecitos Boiling Water Reactor (VBWR) and other facilities to improve the technological limits of boiling water reactors in the following areas:

Task A

1. Extend fuel life information on oxide fuel at high specific power operation and raise the performance limits of oxide fuels.
2. Study power stability and performance characteristics of an oxide-fueled core under natural and forced circulation to improve design limits.

Task B

Conduct out-of-pile experiments in heat transfer and fluid dynamics in the areas of burnout heat transfer, steam void observational studies, and two-phase pressure drop to support in-core work.

Task C

Study long-term reactivity and isotopic composition changes for fuels having lattice characteristics of large power reactors.

This report is written in partial fulfillment of contract AT(04-3)-189, Project Agreement No. 11, Fuel Cycle Program, between the United States Atomic Energy Commission and the General Electric Company. Prior reports to the Commission under this contract have included the following:

1. GEAP-3516, First Summary Progress Report, March 1959 - July 1960.
2. GEAP-3558, First Quarterly Progress Report, August - September 1960.
3. GEAP-3627, Second Quarterly Progress Report, October - December 1960.
4. GEAP-3628, Prediction of Two-Phase Flow From Mixing Length Theory, S. Levy, December 27, 1960. Revision I, May 31, 1961.
5. GEAP-3709, Third Quarterly Progress Report, January - March 1961.
6. GEAP-3655, Pressure Drop Along a Fuel Cycle Fuel Assembly, Various Orifice Configurations, E. Janssen and J. A. Kervinen, May 22, 1961.
7. GEAP-3781, Fourth Quarterly Progress Report, April - June 1961.
8. GEAP-3794, Plan for VBWR Stability Experiment, W. H. Cook, et al., August 30, 1961.
9. GEAP-3835, Fifth Quarterly Progress Report, July - September 1961.
10. GEAP-3898, Sixth Quarterly Progress Report, October - December 1961.
11. GEAP-3953, Seventh Quarterly Progress Report, January - March 1962.
12. GEAP-3766, Critical Heat Flux and Flow Pattern Characteristics of High Pressure Boiling Water in Forced Convection, F. E. Tippets, April 1962.

13. GEAP-3961, Prediction of the Critical Heat Flux in Forced Convection Flow, S. Levy, June 20, 1962.

14. GEAP-4048, Eighth Quarterly Progress Report, April - June 1962.

15. GEAP-4061, Water Surface Waves in Boiling Water Reactors, C. L. Howard and R. G. Hamilton, August 31, 1962.

16. GEAP-4094, Ninth Quarterly Progress Report, July - September 1962.

17. GEAP-4098, Evaluation of Zirconium 1.5 W/O Niobium Cladding for Use in Boiling Water Environments, C. J. Baroch and W. C. Rous, October 1962.

18. GEAP-4107, Heavy Element Isotopic Analysis of UO_2 Fuel Irradiated in the VBWR, Report No. 1, M. R. Hackney and C. P. Ruiz, December 1962.

19. GEAP-4159, Tenth Quarterly Progress Report, October - December 1962.

20. GEAP-3899, Burnout Conditions for Single Rod in Annular Geometry, Water at 600 to 1400 psia, E. Janssen and J. A. Kervinen, February 1963.

21. GEAP-4203, Methods for Improving the Critical Heat Flux of BWR's, C. L. Howard, March 1963.

22. GEAP-3653, AEC Fuel Cycle Program, Design and Fabrication of the Basic Fuel Assemblies, C. J. Baroch, J. P. Hoffman and W. C. Rous, March 1963.

23. GEAP-4206, Evaluation of the Failed BMI Hot Gas Isostatic Pressed Fuel Rods, C. J. Baroch, C. B. Boyer and S. W. Porembka, March 1963.

SUMMARY

Task A - Advanced Fuel Power - Limit Tests

1. Fuel irradiations in the VBWR were resumed with reactor criticality on January 16, and power operation on February 4, 1963. Even though reactor shutdowns were required for location and removal of five failed fuel assemblies (HPD Program), the increase in fuel exposure has been good. The March 24, 1963 exposure status is as follows:

Designation and Clad	Number	Burnup, MWD/T		
		Average of Group	Average for Lead Assembly	Peak for Lead Assembly
H - Annealed stainless (Control rod follower)	10	5,191	6,231	10,280
I - Cold worked stainless	16	4,564	5,803	9,560
J - Zircaloy	24	3,849	6,176	10,200
L - Special fuel	10	-	4,592	7,570

2. Fuel exposures will in the next three months, pass the values at which cold worked stainless steel cladding has been failing under the HPD Program. This will permit tentative evaluation of the effects of the various fabrication and operating variables.

3. Topical reports have been completed titled AEC Fuel Cycle Program - Design and Fabrication of the Basic Fuel Assemblies and Evaluation of Failed Hot Gas Isostatic Pressed Fuel Rods. The content of these reports has been summarized in previous quarterly reports.

4. Failure of the 0.005-inch cold worked stainless steel clad fuel rods in assembly 8L has been traced to strain cycling fatigue. Photomicrographs show that the failures were predominantly transgranular. Four rods were replaced with rods of 0.005-inch annealed stainless cladding.

5. A study of tapered fuel rods indicates a potential advantage for use of a variable water/fuel ratio along the flow channel. The concept is not being further developed in this program because of budget limitations.

6. Natural circulation tests in the hydraulic stability loop have been conducted over a range of conditions from stable, to oscillatory with exponential decay, to self-sustaining oscillations of constant amplitude, to unstable oscillations with divergent amplitude. The oscillations at about 0.4 cps are recorded on all the pressure and velocity instruments. The response to impulses in power input shows the effect of the time delay for transporting steam voids up through the riser. The data permits calculation of oscillation frequency, damping coefficient, time lags, and shows the magnitude and character of pressure and velocity changes.

Task B - Heat Transfer and Fluid Dynamics

1. A topical report, Burnout Conditions for Single Rod in Annular Geometry, Water at 600 to 1400 psia, has been prepared. The data, which has an experimental scatter of ±10 percent

maximum, shows that burnout heat flux: (a) decreases with increasing flow up to 2×10^6 lb/hr-ft^2; (b) has a maximum for hydraulic diameter between 0.25 and 0.5 inch; and (c) decreases for pressure increases between 600 to 1400 psi. A correlating equation for the data is given. The data is compared to results of other investigators. Tests of special geometries show that the burnout heat flux: (a) decreases 22 to 50 percent when the heated rod is within 0.033 inch of the channel wall; (b) is unchanged upstream of a plate-type spacer; (c) decreases 35 to 50 percent when the rod surface is roughened by sandblasting; (d) is increased 20 to 40 percent by use of a "rough liner", i.e., ridges on the unheated channel wall.

2. The four-rod test section is operating satisfactorily and 17 critical heat flux data points have been obtained at 1000 psia and flows of 0.5, 1.0, and 1.5×10^6 lb/hr-ft^2. In each case the critical heat flux occurred at the exit end and on the side of the rod facing the corner of the channel.

3. A topical report, Methods for Improving the Critical Heat Flux for BWR's, includes the evaluation of "film trippers" (rough liner) on the unheated channel walls and indicates considerable promise for increasing the burnout heat flux limit. The theory of operation is that the liquid film on the unheated wall is sheared off and dispersed, thus adding to the liquid film on the heated rod.

4. Measurements with a heater rod bowed so that it is in contact with the channel wall show that the critical heat flux is decreased by a factor of two or more from values with normal clearance. Temperature measurements on the rod, when operating past the critical heat flux, were in the order of magnitude of 1000 F for heat fluxes of about 500,000-600,000 Btu/hr-ft^2.

Task C - Experimental Physics

Chemical analyses for radial variations in isotopic composition within a fuel pellet are nearly completed and have been compiled for interpretation.

TASK A - ADVANCED FUEL POWER-LIMIT TESTS

Irradiation in VBWR

This task provides for irradiation of the special and basic fuel assemblies in VBWR. Summaries of the operating and core loading schedules for the next three months are shown in Tables I and II.

Fuel irradiations in the VBWR were resumed. The core was loaded to a critical configuration on January 16, 1963, and power operation was begun on February 4, 1963, after replacement of the vessel head seal ring, completion of critical tests for control rod worth, and measurements of flow rate in individual fuel channels. The power level was initially limited by several shakedown problems associated with startup from a prolonged outage. The turbine driver for recirculation pump No. 2 was inoperative, which reduced the power capability of the present core to 30 MWt. Also, a very high rate of activity release, presumably from a failed fuel assembly, limited the power level because of high activity in the ventilation exhaust air which is discharged through the old stack. Re-routing the condenser off-gas from the old stack to the new VESR stack has resulted in operation at a factor of ten gain in activity release rate. This is shown in the following table:

	Old Stack	New (VESR) Stack
Effluent	Ventilation	Off-Gas
Discharge Limit for stack	1,000 μc/sec	250,000 μc/sec
Data for last week in February	$<$ 1,000 μc/sec	10,000 μc/sec

A further gain appears to be possible through installation of a system for removal of radioactive material from the ventilation air prior to discharge to the stack. A design study on such a system is in progress.

The reactor was shut down on February 27, when the ventilation exhaust activity increased to the point that reactor power was limited to 10 MWt. Procedures for locating the failed fuel were initiated and three failed fuel assemblies were located and removed. Reactor operation was continued until March 24, when two more suspected failures were removed. The failed assemblies are described in reports of the HPD program (1, 2, 3).

By June, 1963, the basic fuel assemblies of the Fuel Cycle Program will exceed the exposures at which many of the HPD stainless steel clad assemblies have failed. At that time, tentative conclusions about the relative life times of fuel fabricated by different processes can be reached.

BASIC FUEL PROGRAM

The basic fuel program includes the irradiation and examination of a large number of stainless steel and Zircaloy clad fuel assemblies operated at high specific power to long life in a boiling water reactor.

TABLE I

VBWR OPERATING SCHEDULE

February 4, 1963 to April 28, 1963	Power Operation
April 28, 1963 to May 4, 1963	Shut down. Revise fuel loading.
May 5, 1963 to June 2, 1963	Power Operation
June 2, 1963 to June 9, 1963	Shutdown
June 10, 1963 to July 14, 1963	Power Operation

TABLE II

VBWR CORE COMPOSITION

	Fuel Elements in Core			
	March 31	April 30	May 31	June 30
Fuel Cycle				
A-2 Basic	13	13	11	11
A-2 Special	6	6	9	9
A-1 Driver	34	34	35	35
	53	53	55(a)	55
Consumers HPD	23	23	24	23
Plutonium	1	1	1	1
Dresden	2	2	2	2
APED General Development	1	1	0	0
Savannah I	3	3	3	3
Savannah II	5	5	5	5
ESADE	4	4	4	4
Test Assemblies	92	92	94	93
APED Drivers				
Rod	20	20	15	15
Plate	6	6	9	10
Total Fuel	118	118	118	118

(a) Fuel moves at next scheduled core arrangement (April 28 - May 4) are: add 1I, 25J, 1L, 8L, and 11L, which have had defect rods replaced with sound rods, remove 8J, 6I, and 11I, and change 17J from A-2 to A-1 status. This places all Fuel Cycle assemblies in core except 8J, 6I, 11I and 4L. Assembly 23J is counted under the Plutonium Recycle (PA No. 23) Program.

The status of the 50 assemblies is listed in Table III, and summarized below:

Designation and Clad	Number	Burnup, MWD/T[1] Average of Group	Burnup, MWD/T[1] Average for Lead Assembly[2]
H - Annealed stainless (Control rod follower)	10	5,191	6,231
I - Cold worked stainless	16	4,564	5,803
J - Zircaloy	24	3,849	6,176

(1) Burnup, at end of run No. 155 which was completed on March 24, 1963.

(2) Peak exposure is about 1.65 times this value.

At the request of the AEC, the irradiation of assemblies 6I, 11I and 8J will be terminated during the next VBWR core rearrangement. Also, 17J will be changed from an A-2 to an A-1 assembly.

To provide the maximum assurance of continued high power operation of the VBWR, irradiation of intentionally defected fuel rods has been postponed. Consequently, assemblies 1I and 25J, which contain defected fuel rods, were not irradiated this quarter. The defected fuel rods in 25J were replaced with nondefected fuel rods when the fuel rods were transferred to a new frame which incorporates constant pressure spring clip spacers to reduce the problem of fretting. Visual inspection of the fuel rods during the transfer operation revealed that fretting wear has not been serious enough to prevent the continued irradiation of the fuel rods. The defect rod in assembly 1I will be replaced with a nondefected fuel rod and the irradiation of assemblies 1I and 25J will be resumed after the next VBWR core rearrangement.

The topical report, AEC Fuel Cycle Program - Design and Fabrication of the Basic Fuel Assemblies, GEAP-3653, by C. J. Baroch, J. P. Hoffmann, and W. C. Rous, dated March 15, 1963, has been completed.

TABLE III

BASIC FUEL IRRADIATIONS

STAINLESS STEEL CLAD ASSEMBLIES

Assembly Number	Specific Power (1) Kw/Kg	Heat Flux(1) Btu/hr-ft^2 × 10^{-3} Average	Peak	Accumulated Exposure MWD/T
1H	19.6	125	216	4069
2H	20.9	132	229	4217
3H	24.0	151	261	4804
4H	32.2	202	345	5867
5H	26.9	168	307	5160
6H	21.8	137	251	4868
7H	27.9	176	293	5194
8H	26.6	172	295	5401
9H	34.4	217	367	6231
10H	26.4	166	282	5100
1I	(2)	(2)	(2)	4675
2I	27.9	180	297	3813
3I	20.7	133	243	4816
4I	26.6	170	280	4836
5I	16.8	108	181	4052
6I	29.2	189	328	4865
7I	16.1	104	168	4221
8I	36.6	237	405	5764
9I	33.0	214	346	5803
10I	21.4	138	253	4652
11I	22.7	147	276	5184
12I	18.2	117	205	4431
13I	24.8	160	285	4327
14I	23.7	152	250	4789
15I	14.9	95	168	1709
16I	28.3	182	305	5079
1J	21.7	136	246	3826
2J	18.1	113	208	3085
3J	17.0	103	195	3165
4J	23.3	146	267	3861
5J	26.5	167	273	4342
6J	37.0	234	380	4702
7J	23.3	147	266	3873
8J	26.9	169	291	4147
9J	25.7	162	285	4342
10J	19.3	122	205	3481
11J	34.4	217	360	6176
12J	37.5	237	382	6069
13J	34.2	216	347	5891
14J	30.9	196	303	5328
15J	25.4	164	270	3491
16J	31.5	199	328	4245
17J	28.2	178	316	3182
18J	32.0	202	335	3218
19J	17.3	109	190	2958
20J	11.7	74	136	3109
21J	21.1	113	216	2519
22J	26.7	167	300	2841
23J	23.0	144	267	2334
25J	(2)	(2)	(2)	2187

(1) Peak condition during this quarter.
(2) Not irradiated this quarter.

SPECIAL FUEL PROGRAM

The Special Fuel Program includes the irradiation and examination of 12 fuel assemblies based on fuel concepts which show potential for improved fuel cycle economy through increased performance or lower fabrication costs. These assemblies will be operated at high specific power to long life to determine performance capabilities in relation to the basic fuel assemblies which represent current fuel design and fabrication processes. Some of the special fuel assemblies represent engineering proof tests of fuel concepts which have been developed by other Atomic Energy Commission contractors. The status of the special assemblies is summarized in Table IV.

1. Higher Thermal Performance

   Operation of fuel at higher thermal performance improves the economics of the fuel cycle, provided that a reasonable fuel lifetime is achieved. Assembly 1L is a test of UO_2 fuel life at higher temperatures while assembly 9L provides an evaluation of thermal conductivity improvers.

   a. Centermelt - Assembly 1L

      Assembly 1L is being operated in the VBWR to evaluate the lifetime performance of UO_2 operated near the point of UO_2 centermelting.

      Because the 1L assembly contained one defected rod, the assembly was not irradiated during this quarter. However, the defect rod will be replaced with a nondefected rod and the irradiation will be resumed during the next VBWR run.

   b. Centermelt Calibration Rod

      The analysis of the centermelt calibration rod has been completed. Information regarding the examination of the centermelt calibration rod is reported in the Seventh, Eighth, and Ninth Quarterly Progress Reports, GEAP-3935, GEAP-4048, and GEAP-4094, respectively. A topical report which discusses the results of the analyses is in the final stages of preparation.

   c. Improved Thermal Conductivity - Assembly 9L

      If the thermal performance of UO_2 is limited by centermelting or fission gas release at high temperatures, there might be advantages in improving the thermal conductivity of the fuel by addition of thermal conductivity improvers. Assembly 9L uses molybdenum (15 to 20 weight percent) dispersed throughout the UO_2. Two methods of dispersion are being investigated: one approach is to mix molybdenum fibers with UO_2 powder prior to pressing of the pellets; the other approach is to coat the individual UO_2 particles with molybdenum metal prior to the pressing of the pellets.

      This assembly has accumulated an average exposure of 907 MWD/T at a peak heat flux of 385,000 Btu/hr-ft^2 and continues to operate satisfactorily.

TABLE IV

STATUS OF SPECIAL FUEL ASSEMBLIES

Element	Concept	Specific Power[1] kw/kg	Heat Flux[1] Btu/hr-ft^2 × 10^{-3} Average	Heat Flux[1] Btu/hr-ft^2 × 10^{-3} Peak	Accumulated[2] Exposure MWD/T
1L	Centermelt	(3)	(3)	(3)	4075
4L	Low temperature sintered pellets	(3)	(3)	(3)	234
5L	Co-extruded UO_2 and stainless steel clad	33.9	223	364	4592
6L	Zircaloy-4 clad	16.8	145	287	1075
7L	Stainless steel lined Zr-2	35.6	224	383	4303
8L	0.005-inch stainless steel clad pellets	(3)	(3)	(3)	2553
9L	Thermal conductivity improver	30.9	233	385	907
10L	0.005-inch stainless steel clad over powder	19.2	116	211	396
11L	Extruded UO_2	(3)	(3)	(3)	180
12L	Burnable poison	15.4	110	191	307
2L	Undefined	-	-	-	-
3L	Undefined	-	-	-	-

(1) Peak condition during this quarter.

(2) Exposures are through VBWR run No. 155 which was completed on March 24, 1963.

(3) Not irradiated this quarter.

2. Reduced Cladding Parasitic Absorption Concepts

Zirconium alloys provide a low neutron cross section fuel element cladding for use in pressurized and boiling water reactors. The Zircaloys have good corrosion resistance to water at temperatures normally encountered in these reactors. These alloys may, however, be susceptible to hydride embrittlement and severe corrosion damage, particularly on the inside surface of the cladding if water enters the fuel rod. The austenitic stainless steels also have good corrosion resistance in high temperature water and should be somewhat less susceptible to severe corrosion damage on the inside surface of the clad of defective fuel rods. Austenitic stainless steels, however, have an appreciable thermal neutron cross section. One mil of thickness of stainless steel has about the same macroscopic cross section as 30 mils of thickness of Zircaloy.

The approaches to reduced parasitic absorption in the fuel cladding being pursued are to: (1) improve the corrosion resistance of zirconium alloys; (2) provide protection to the inside surface of commercially available zirconium alloys such as Zircaloy-2; and (3) reduce the thickness of the stainless steel clad to that of a thin corrosion skin rather than a pressure tube. At least one special assembly is devoted to the evaluation of each of the above concepts.

a. Zircaloy-4 Clad - Assembly 6L

The fuel rods in assembly 6L contain UO_2 pellets clad with Zircaloy-4. The defect rod in this assembly was replaced with a nondefect rod and the irradiation of this assembly was resumed in February, 1963.

b. Stainless Steel Lined Zircaloy-2 - Assembly 7L

Assembly 7L consists of fuel rods containing UO_2 pellets clad with Zircaloy-2 lined on the inside with about 1.0 to 1.5 mils of type 304 stainless steel. The assembly has accumulated a burnup of 4303 MWD/T and continues to operate satisfactorily.

c. Thin Walled Stainless Steel Tubing - Assemblies 8L and 10L

The fuel rods in assembly 8L contain UO_2 pellets clad with 0.005-inch thick stainless steel tubing. The detailed RML examination of the four damaged or failed fuel rods has been completed. The RML examination revealed the following:

Rod 502: The clad from this rod contained a wrinkle in the plenum area. There was a longitudinal crack about one-half inch long at the crest of the wrinkle. This rod was measured, then sectioned through the crack and the clad removed from the plenum support tube. Diametral measurements of the clad during the examination indicated the following:

Outside diameter at the crest of the wrinkle	0.400 inch
Outside diameter at 90 degrees from wrinkle	0.376 inch
Outside diameter of plenum support tube	0.363 inch

The analyses of these measurements are presented in the discussion of rod 538.

A section of the clad from the plenum, which was mounted for metallurgical examination, was not examined because information obtained from the examination of rods 514 and 538 would not be significantly supplemented.

Rod 509: Ultrasonic inspection indicated that this rod contained a defect in the peak flux region. However, the crack could not be located by visual examination or by pressurizing the inside of the fuel rod with helium under water. The scope of any additional examination of the fuel rod has not been determined.

Rod 514: This rod contained a longitudinal crack about one inch long in the peak flux region. The rod was sectioned through the crack for detailed examination. A photograph of the cross section through the failure is shown in Figure 1; photomicrographs of the failure are shown in Figures 2 and 3. The heavy concentration of precipitates are believed to be silicates; they are not carbides or sigma phase. These precipitates were present in the as-received tubing.

Diameter measurements on the rod at the peak heat flux location indicate a uniform increase of 2 ±1 mils as a result of operation. Pre-cut measurements indicate the diameter at the crack was approximately 0.5 mil greater than the diameter measured 90 degrees from the crack. The loss of UO_2 which can be seen in Figure 1 occurred during sectioning. Also, the severe clad peak at the crack in Figure 1 was apparently exaggerated by sectioning.

During the irradiation of the assembly, there were 71 power cycles and 126 thermal cycles. A power cycle is defined as a change in VBWR power from 5 MWt to more than 20 MWt and return. A thermal cycle is defined as a change in power from less than 2 MWt to 5 MWt and return.

The cause of cracking of this rod is apparently strain cycling fatigue. The differential thermal expansion of the UO_2 and clad during operation of the fuel rod at the peak heat flux condition, about 500,000 Btu/hr-ft^2, would have caused a calculated plastic diametral deformation in the clad of 0.002 inch. When power is reduced after plastic strain of the clad, the contraction of the UO_2 leaves an equivalent gap between the clad and UO_2. If the gap is as large as these calculations indicate, there is high probability that collapse under the 1000-psig coolant pressure would have caused a wrinkle. Repeated cycling of this wrinkle after formation probably led to fatigue cracking. Metallurgical examination of the clad crack supports this conclusion. Figures 2 and 3 are photomicrographs of the fracture, which is predominantly transgranular. The diamond pyramid hardness of the clad in the failure and at 180 degrees from the failure are listed in Table V. The clad in the failure region appears to be slightly harder than the clad in the nonfailure region. This increase in hardness may be caused by work hardening during the cycling.

The tensile properties of the nonirradiated clad and the clad from the vicinity of the failure are reported in Table VI. Because of the nonuniformity in clad thickness, the variations in the yield strength and ultimate tensile strength are expected. There is,

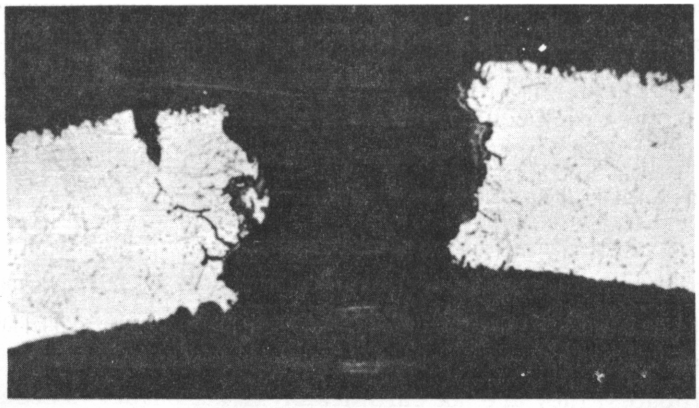

ETCHED 250X

1150–2

Figure 1. Cross Section of Rod 514 at the Failure in the Peak Heat Flux Region

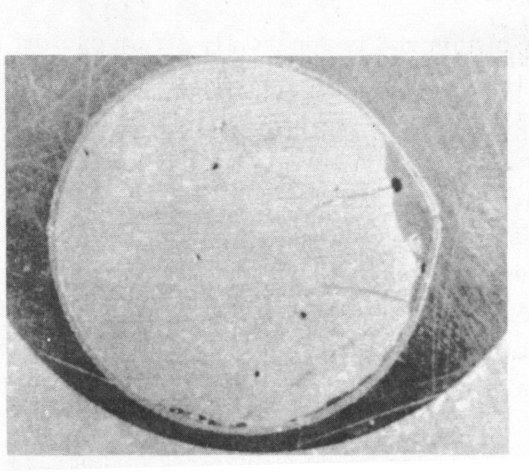

AS GROUND 7X

1150–1

Figure 2. Photomicrograph of the Failure in Rod 514

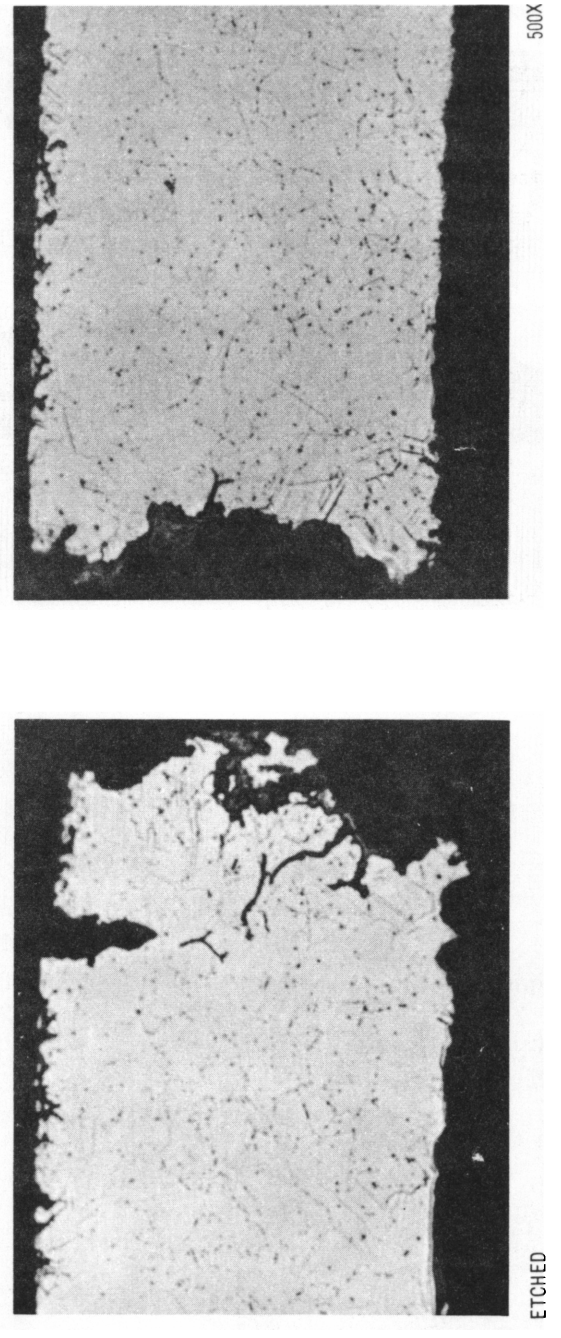

Figure 3. Photomicrograph of the Failure in Rod 514

TABLE V

DIAMOND PYRAMID HARDNESS OF 8L IRRADIATED CLAD

Location of Measurement	DPH (0.1 Kg load)		
	Overall Average	Inside Surface	Outside Surface
Failure Area	252	253	254
Nonfailure Area	239	234	246

TABLE VI

ROOM TEMPERATURE TENSILE PROPERTIES OF 8L CLAD

Specimen Number	Fast Flux, nvt (>1 mev)	Yield Strength psi	Ultimate Strength psi	Elongation Percent
1	2.3×10^{20}	94.6	108.8	4.9
2	2.3×10^{20}	93.3	102.0	3.8
3	0	86.7	121	29.0
4	0	91.3	120	27.5

however, a very noticeable decrease in percent elongation after irradiation. The other tensile properties and hardness are not affected by the short irradiation. Consequently, the cause of this loss in ductility remains unexplained.

Rod 538: The clad in this rod was severely wrinkled in the plenum. A section through this wrinkle is shown in Figure 4. The analyses of this photograph and other available data revealed the following:

OD of the rod at the crest of the winkle	0.401 inch
OD of the rod at 90 degrees from the wrinkle	0.377 inch
OD of the plenum support tube	0.365 inch
Initial OD of the rod	0.376-0.383 inch
Initial diametral gap estimated from OD of as-fabricated rod and diameter of plenum support tube (0.365-inch)	0.000-0.008 inch
Initial diametral gap estimated from area in the bulge	0.0025 inch

Previous work at APED indicates that wrinkling of this clad would be expected with a diametral gap of this size. The large initial diametral gap was probably caused by the diameter of the plenum support tube being too small and the cold swaging operation not reducing the gap in the plenum as much as predicted. (During fabrication, the clad was cold swaged to reduce the gap between the clad and pellets or plenum support tube.)

Assembly 8L, in which the four failed rods were replaced with fuel rods clad with annealed 0.005-inch thick stainless steel, was not irradiated during this quarter because it contained a defect rod. The defect rod has been replaced and the irradiation of the assembly will be resumed during the next VBWR run.

Assembly 10L contains vibratory compacted UO_2 powder clad with 0.005-inch thick stainless steel tubing. The irradiation of the assembly began in February, 1963. The VBWR license requires that a new assembly must be irradiated, initially, in a core location where the peak heat flux is $<250,000$ Btu/hr-ft^2. If the assembly is satisfactory according to visual examination after the initial operation, then it will be moved to a core location where the peak heat flux is $>400,000$ Btu/hr-ft^2.

3. High UO_2 Density and Reduced Fabrication Cost Concepts

Irradiation of assemblies containing fuel rods made by new fabrication processes, which offer potential increases in UO_2 density or cost reductions in the manufacture of UO_2 fuel elements, will provide engineering proof tests of the feasibility of these new methods. The testing of fuel rods fabricated by the following methods is in progress or has been completed:

a. Isostatic gas pressing - Assembly 4L
b. Low temperature sintered pellets - Assembly 4L
c. Co-extruded UO_2 and stainless steel clad - Assembly 5L
d. UO_2 extrusions - Assembly 11L

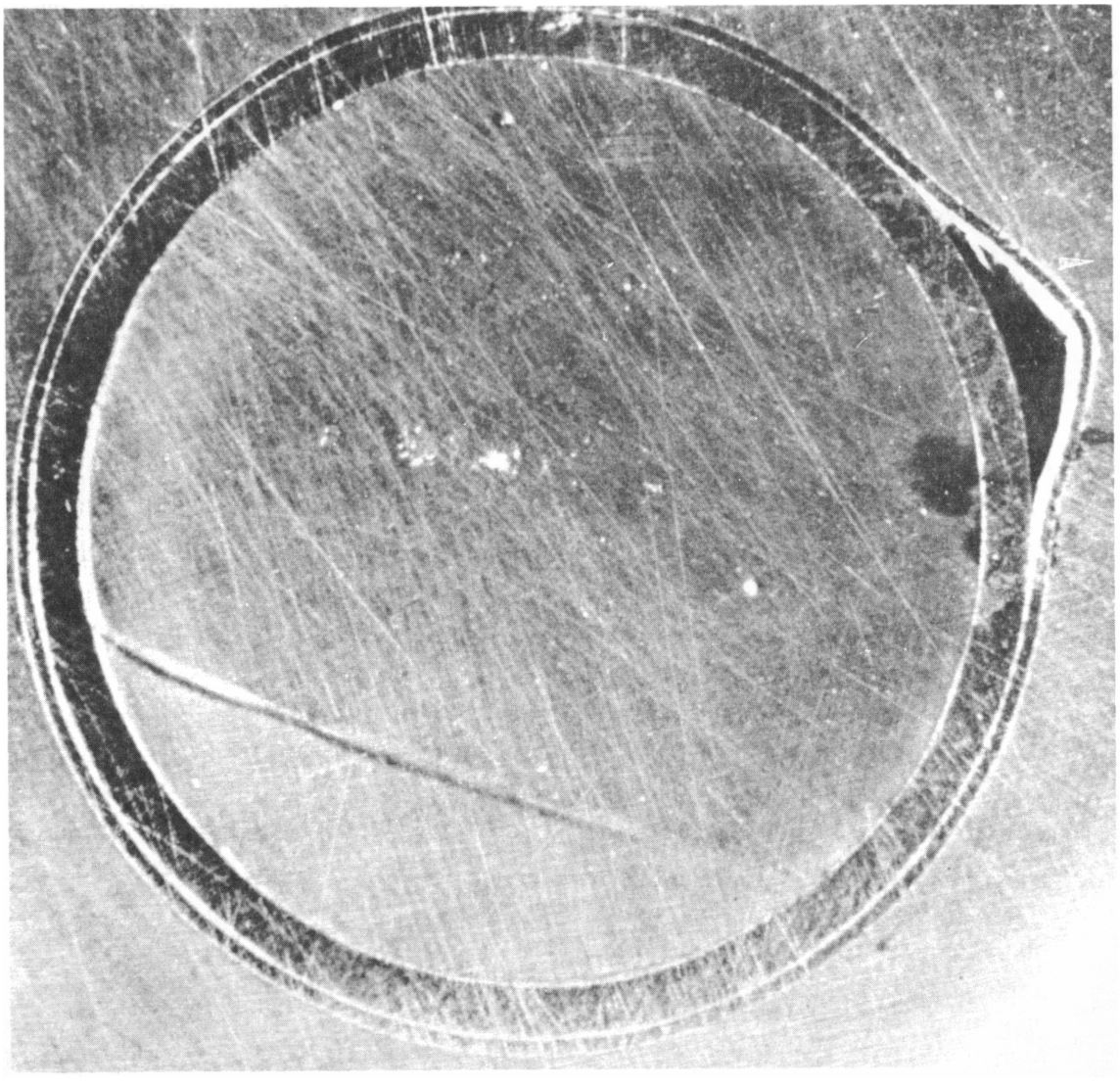

COARSE POLISH 18.5X

1150–4

Figure 4. Profile of Wrinkle in Plenum of Rod 538

a. Hot Gas Isostatic Pressed - Assembly 4L

Several fuel rods were fabricated at BMI by hot gas isostatic pressing (gas pressure bonding) of the UO_2 and stainless steel clad. The three fuel rods which were irradiated in the VBWR failed after an average exposure of 316 MWD/T. The results of the examination are reported in GEAP-4206, Evaluation of Failed Hot Gas Isostatic Pressed Fuel Rods, by C. J. Baroch of General Electric and C. B. Boyer and S. W. Porembka of BMI, which was completed during March, 1963. The content of this report was summarized in the Tenth Quarterly Progress Report, GEAP-4159. The publication of this report thus completes the evaluation of the hot gas isostatic pressed fuel rods.

b. Low Temperature Sintered Pellets - Assembly 4L

Among the 16 fuel rods in assembly 4L are three fuel rods containing low temperature sintered UO_2 pellets. These fuel rods were fabricated by the United Nuclear Corporation using a low temperature sintering process for the preparation of the UO_2 pellets.

Assembly 4L was not irradiated during this quarter because it contains two defected fuel rods. Furthermore, the irradiation of the assembly has been terminated at the request of the AEC. Because of the continued interest in the fuel rods containing the low temperature sintered pellets, these fuel rods will be transferred from assembly 4L to assembly 5L following the present VBWR run (about April 28).

c. Co-Extruded UO_2 and Stainless Steel - Assembly 5L

Twelve fuel rods in assembly 5L were manufactured at Nuclear Metals, Inc., by co-extruding the UO_2 fuel and the stainless steel clad. Assembly 5L was irradiated during this quarter and continues to operate satisfactorily. After the next VBWR run has been completed, three of the co-extruded fuel rods will be replaced with the three fuel rods containing the low temperature sintered pellets from assembly 4L.

d. UO_2 Extruded Fuel - Assembly 11L

Assembly 11L is composed of six fuel rods containing Allis Chalmers UO_2 extrusions, six fuel rods containing CICAF UO_2 extrusions, and four rods containing UO_2 pellets. Because the assembly contains two defected fuel rods, it was not irradiated during this quarter. The two defected fuel rods will be replaced with nondefected fuel rods containing UO_2 pellets and the irradiation of the assembly will be resumed with the next VBWR run.

4. Extended Life Concepts

The loss of reactivity as the result of fuel burnup may limit the lifetime of the fuel. Initial reactivity for burnup is limited by the capacity of the control system to make the cold, clean core subcritical. The reactivity change associated with fuel burnup can be reduced by burnable poisons. Assembly 12L contains fuel rods which contain boron as a burnable poison by: (1) alloying small quantities of boron with the stainless steel cladding, and (2) by mixing the boron compound with UO_2. The irradiation of assembly 12L began in February,

1963. The VBWR license requires that a new assembly be irradiated in a core location where peak heat flux is $<250,000$ Btu/hr-ft^2. After the initial operation, the assembly will be visually inspected. If no defects are evident during the visual examination, the assembly will be moved to a core location where the peak heat flux is $>400,000$ Btu/hr-ft^2.

5. Study of Tapered Fuel Rods for Use in Large BWR's

The purpose of this preliminary study was to determine if there was sufficient incentive for tapered fuel rods to justify fabricating and irradiating one fuel bundle in the VBWR as a special fuel element in the Fuel Cycle Program.

Results indicate that the tapered fuel rod might provide:

a. Increased reactivity for a given mass of UO_2
b. Less restrictive control requirements at the top of the core
c. Improved axial power distributions

In an effort to determine the advantages of tapered rods, a few basic parameters were compared to those obtained from a constant diameter rod. The core characteristics assumed are:

Core power density	35 kw/l
Core height	9 ft
Core diameter	9 ft
Subcooling	20 Btu/lb
Exit quality	6 percent
UO_2 enrichment	2.6 percent

The uniform tapered rod varied in outside diameter from 0.475-inch at the core bottom to 0.350-inch at the top. This corresponds to a water-to-fuel-volume ratio range of 1.6 to 4.0. The stainless steel clad thickness was changed along the rod such that the thickness is proportional to the UO_2 diameter.

The constant diameter rod dimensions were chosen such that this rod contained the same UO_2 volume as the tapered rod. This results in a rod diameter of 0.409-inch with a water-to-fuel ratio of 2.6.

Figure 5 shows the axial power and void distribution for the two rods, assuming a uniform square lattice. Each power distribution is normalized to an average of 1.0. The peak-to-average power has been reduced from 2.8 for the uniform rod to 1.9 for the tapered rod. The average void for the tapered rod has been reduced from 36 percent in the uniform rod to 29 percent as a result of the higher position in the core of the power production.

It is significant to note that an increase in reactivity of about 1.4 percent was obtained for the tapered rod. Although not calculated the difference in reactivity resulting from voids might be even more significant. Although the power distribution has been flattened significantly with the tapered rod, it should be remembered that this analysis assumes a uniform lattice with no control. It is expected that both distributions could be improved by judicious

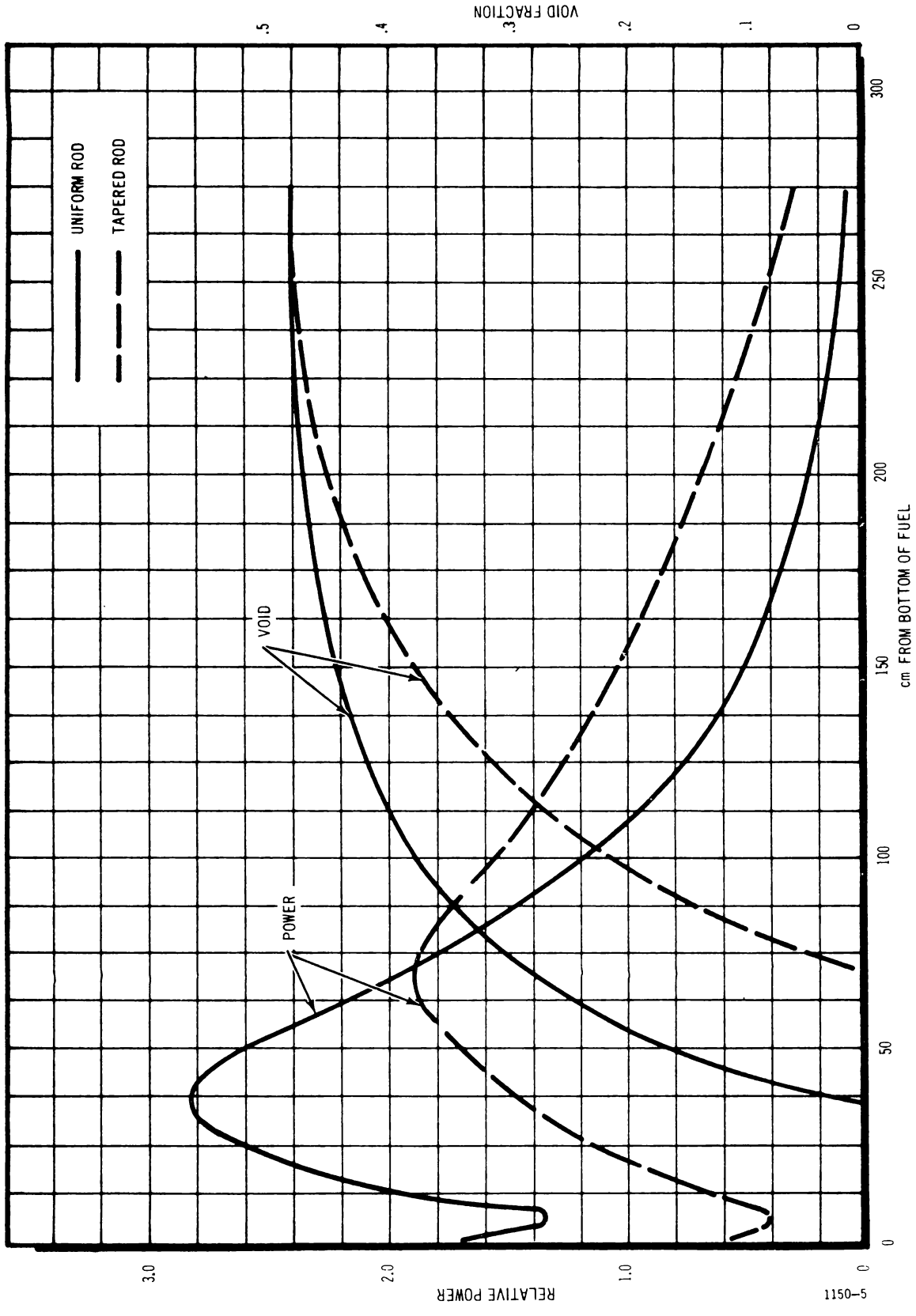

Figure 5. Axial Power and Void Distribution - Tapered Rods

selection of control patterns. It does appear, however, that the tapered rod would offer some incentive for the ultimate best distribution.

Figure 6 shows that the specific power peak has been reduced from 37 kw/kg-U to 22 kw/kg-U in the tapered rod. Figure 7 shows that the tapered rod peak heat flux is considerably lower than that in the constant diameter rod. The heat flux is computed at the outside of the clad. This brief analysis indicates that the tapered rod does have some advantages over the constant diameter rod.

Significant assumptions used in this study which should be kept in mind in evaluating the results are:

a. The lattice was assumed to be horizontally uniform and thus did not include the effects of dead water between the channels. This probably unduly penalizes the straight rods.

b. The effects of control rods and burnup on the power distribution have not been investigated.

c. The significance of these results with regard to the burnout heat flux limit has not been evaluated.

d. The temperature and void coefficients of reactivity and their variation with temperature during startup and with core location, have not been investigated.

The advantages of the tapered rod which are implied from this brief study appear to warrant increased study to determine the significance of the limitations described above.

This study has shown a potential advantage in power distribution achieved by tapered fuel rods. This same advantage could be achieved by several mechanical methods which give a variation in water/fuel ratio over the height of the core. These mechanical arrangements are not necessarily ideal, but are possible within the present technology without the requirement of development work. Such methods include:

a. Decreasing rod diameter in 1 or 2 steps using end plugs and screwed connectors.
b. Decreasing number of rods in upper part of reactor by using several partial length rods in each assembly.
c. Using segmented fuel with decreasing number of rods and/or diameter of rods in upper portions of reactor.

The next step in the development of this concept is the design evaluation of the mechanical alternatives and costs for achieving a variable water/fuel ratio. This must be compared to the cost incentive attributed to the power flattening and increase in core rating achieved. Such a study necessitates some optimization of the variation in water/fuel ratio.

A more detailed evaluation of this type is not being made under this program and a tapered rod fuel assembly is not being fabricated because of manpower and budget limitations. Further evaluation is, however, considered to be desirable.

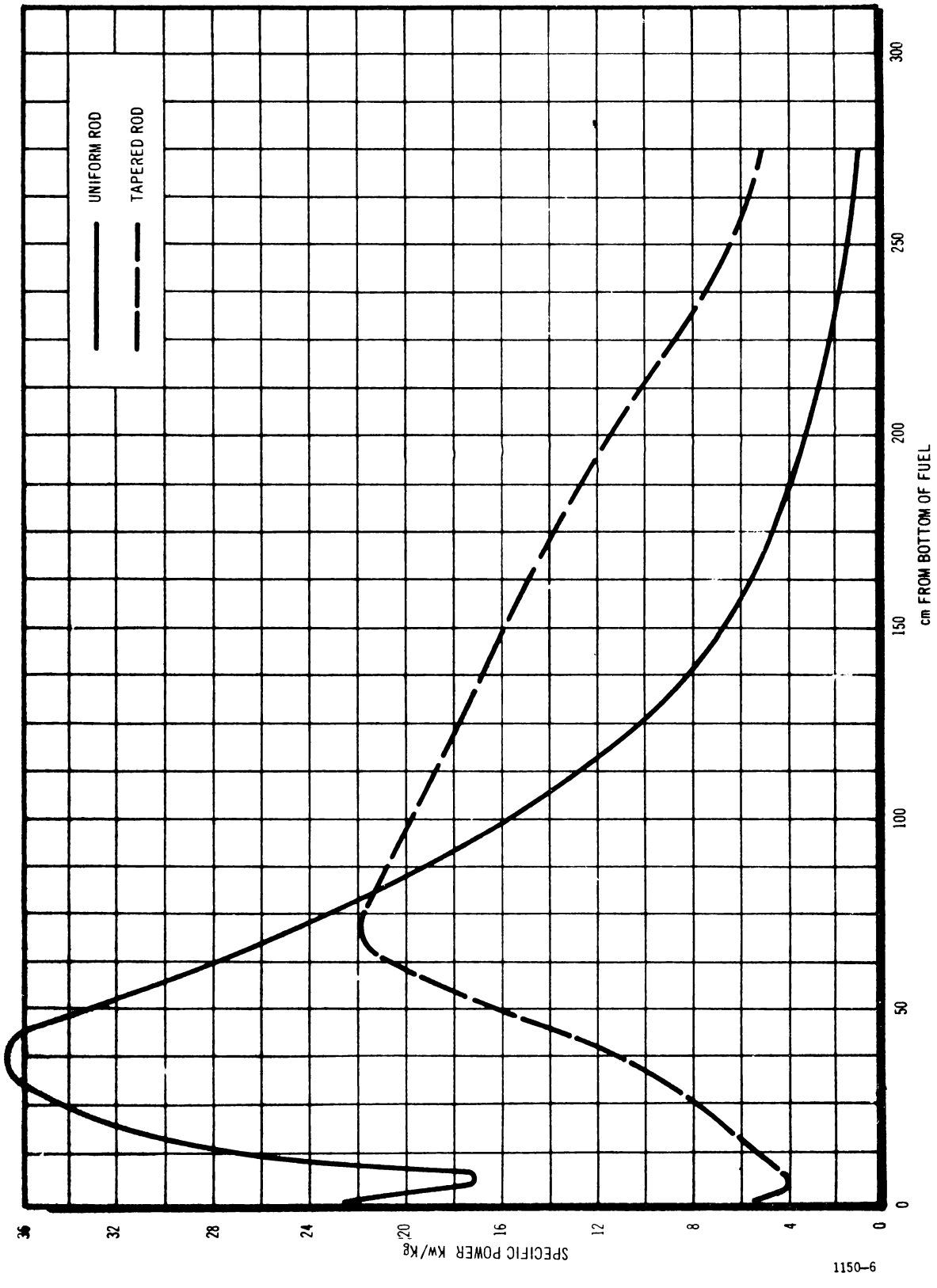

Figure 6. Axial Specific Power Distribution Tapered Rods

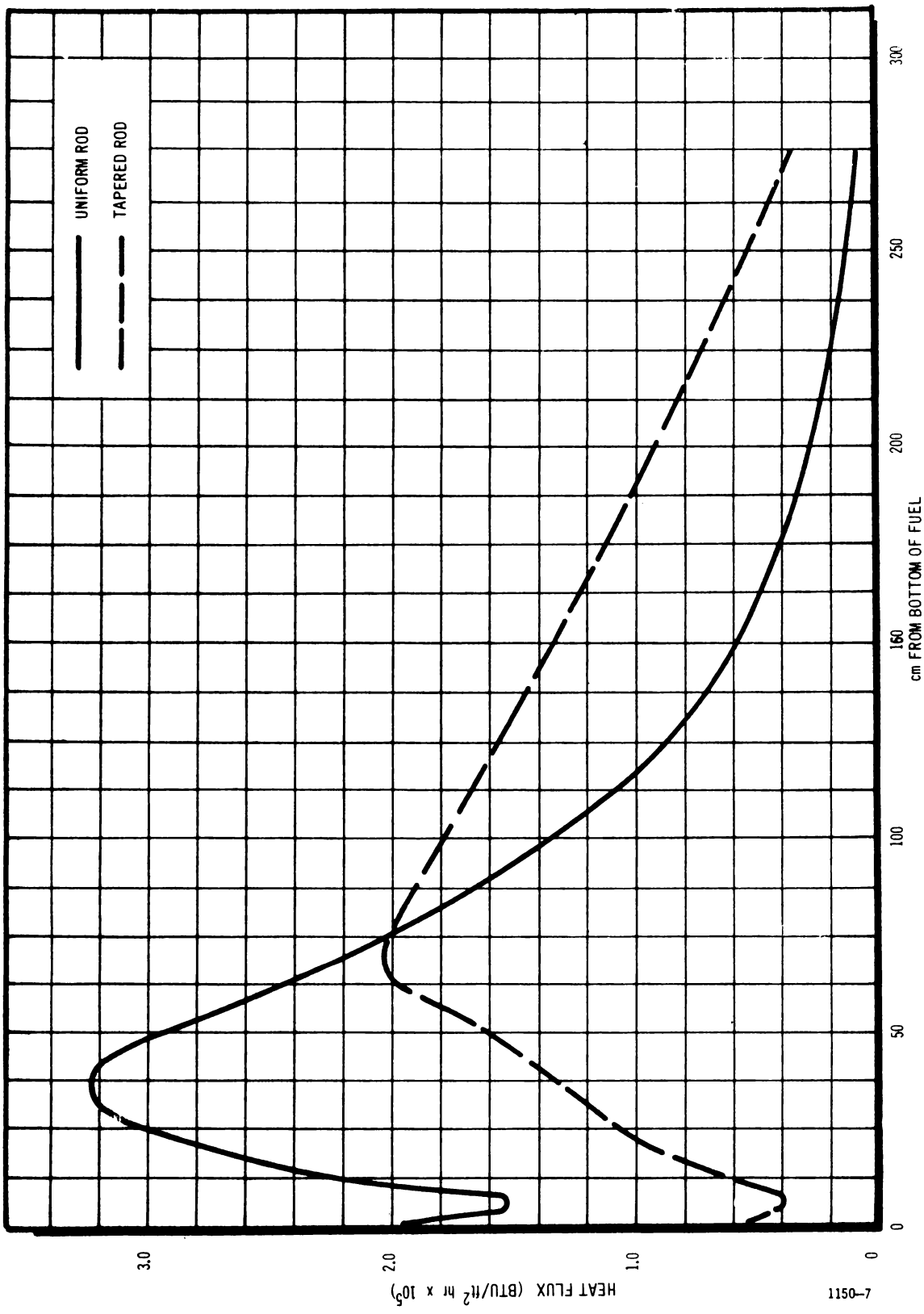

Figure 7. Axial Heat Flux Distribution - Tapered Rods

STABILITY

This task provides for the development of a mathematical stability model to predict the dynamic performance of boiling water reactors, and for a stability test in the VBWR and experiments in a stability loop to provide an experimental basis for the model.

Hydraulic Stability Test Loop

Testing has been continued on the natural circulation operational parameter phase of the program. A total of 45 runs were conducted, including both steady-state and power impulse transient runs. Pressure for the tests was 1000 psi. Natural circulation flow arrangement was used on all tests with the flow system predominantly in a minimum restriction condition.

The tests showed a wide range of oscillatory conditions, ranging from stable, to oscillatory with exponential decay, to self-sustaining oscillation of constant amplitude, to unstable oscillations with divergent amplitude. For the stable condition with low damping, any of the following loop operations triggered oscillations:

1. Opening instrument line with cold water in it,
2. Power impulse or change,
3. Blowdown of water to change water level, or
4. Opening valve in recirculation line.

At each test condition, the following parameters were recorded on an eight-channel recorder:

1. Pressure at the top of the riser,
2. Pressure differential across riser,
3. Pressure at heater outlet (riser inlet),
4. Pressure differential across heater,
5. Pressure at inlet to heater,
6. Velocity at heater inlet,
7. Inlet temperature and
8. Heater current.

Table VII gives a summary of tests conducted from January 28, 1963, to March 5, 1963. In Figure 8, the test range is presented as a plot of subcooling (Δh_s), against quality (x). To test the analytical model, the tests were aimed at obtaining as great a spread in the test range as possible. The two limits are maximum subcooling (limit shown in Figure 8) and minimum subcooling (operational limit of 10-15 Btu/lb). Experimentally, the high subcooling runs were easy to obtain, but the low subcooling runs were obtainable only to about 10 percent quality. Water level changes were made in the steam drum separator (which is related to the water level in the condenser-subcooler system) to achieve low subcooling. These tests were partially successful in extending the low subcooling data. This loop operational problem will be pursued. The water level change tests will also demonstrate the effect of varying the volume of the steam in the steam separator.

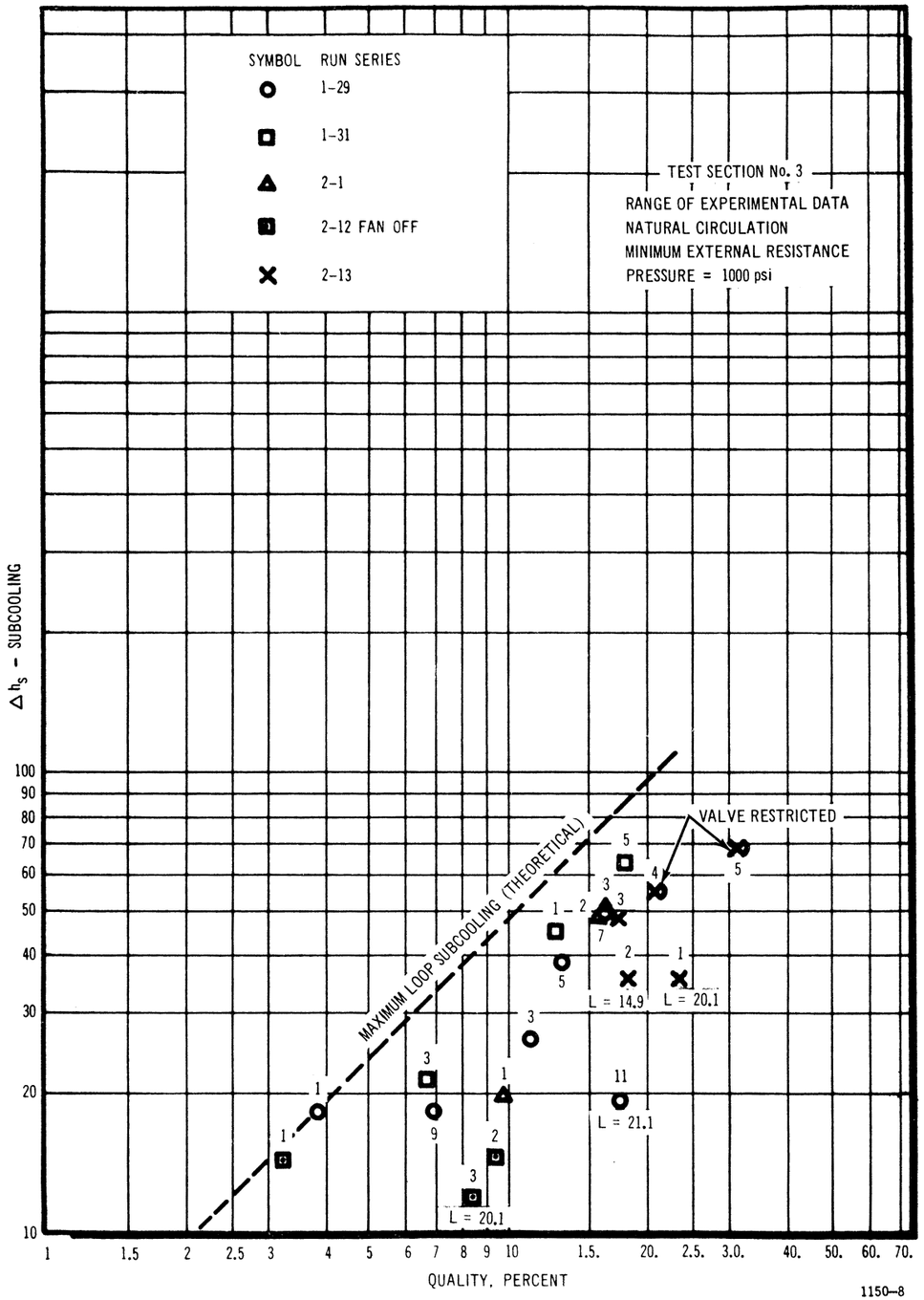

Figure 8. Range of Experimental Data, Hydraulic Stability Loop

TABLE VII

SUMMARY OF TEST RUNS - STABILITY LOOP

RUN NO.	DATE	POWER KW	VELOCITY FT/SEC	QUALITY %	SUB COOLING BTU/lb	LEVEL	FAN ON OR OFF	EXTERNAL RESISTANCE	MODE OF OPERATION	TYPE OF DISTURBANCE	REMARKS
1-28-1	1-28-63							MIN.	NAT. CIR-CULATION		
1-28-2	1-28-63									Negative Power Perturbation	Produced oscillatory flow of about 1/5 cps; oscillation is damped out in about 12 cycles. Pressure drop across test section and riser also oscillate in phase with flow; the absolute pressure oscillations however, are out of phase (about 90 degrees)
1-28-3	1-28-63										
1-29-1	1-29-63	19.33	4.93	3.83	18.3	11.25					
1-29-2	1-29-63	18.38			18.3					Negative Power Perturbation Positive Power	Flow experienced large jump but did not oscillate; i.e., behaved as if critically damped. Same as above, but reversed.
1-29-3	1-29-63	46.0	5.14	11.10	26.3						
1-29-4	1-29-63	46.0			26.3					Positive Power Perturbation	Flow oscillated but damped out rapidly.
1-29-5	1-29-63	55.4	4.96	13.0	38.5	11.75					
1-29-6	1-29-63	55.4			38.5	High Water				Negative Power Perturbation	Flow oscillation damped out in two cycles; i.e., overshot twice (underdamped)
1-29-7	1-29-63	67.3	4.83	16.18	49.1	12.1					
1-29-8	1-29-63	67.3			49.0	Normal Water				Positive Power Perturbation	Flow oscillation damped out in two cycles; i.e., overshot twice (underdamped)
1-29-9	1-29-63	29.2	5.11	6.92	18.3						
1-29-10	1-29-63	29.2			18.3					Positive Power Perturbation	Flow response appeared very close to critically damped; i.e., one slight overshot.
1-29-11	1-29-63	55.7	4.64	17.44	19.3	21.1					
1-29-12	1-29-63	55.7			19.3					Positive Power Perturbation	The flow variation appeared to be critically damped. The response was similar for negative power. Pressure data exhibited the same characteristic as the flow data.
1-31-1	1-31-63	57.1	4.94	12.62	45.7	11.0					
1-31-2	1-31-63										
1-31-3a	1-31-63	29.0	4.96	6.61	21.4	10.6					
1-31-3b	1-31-63										
1-31-4	1-31-63					10.6					
1-31-5	1-31-63										

TABLE VII (Cont.)

RUN NO.	DATE	POWER KW	VELOCITY FT/SEC	QUALITY %	SUB-COOLING BTU/lb	LEVEL	FAN ON OR OFF	EXTERNAL RESISTANCE	MODE OF OPERATION	TYPE OF DISTURBANCE	REMARKS
1-31-6	1-31-63	78.1	4.79	17.8	63.9	10.6		MIN.	NAT. CIR-CULATION		
2-1-1a	2-1-63	37.65	5.01	9.66	19.8	12.6					
2-1-1b	2-1-63	37.65			20.00	12.6				Negative Power Perturbation	Flow oscillation just barely overshot the second time. However, no overshoot was apparent in the ΔP data.
2-1-2a	2-1-63	65.8	4.80	15.67	49.0	11.9					
2-1-2b	2-1-63					11.9					
2-1-3a	2-1-63	68.0	4.80	16.22	50.2	13.0					
2-1-3b	2-1-63					13.0					
2-12-1a	2-12-63	15.03	4.73	3.2	14.2	11.4	OFF				
2-12-1b	2-12-63										
2-12-2a	2-12-63	34.3	5.06	9.35	14.4	12.1	OFF				
2-12-2b	2-12-63										
2-12-3a	2-12-63	30.4	5.06	8.42	11.9	20.1	OFF				
2-12-3b	2-12-63										
2-13-1a	2-13-63	74.0	4.36	23.4	35.5	20.1	ON				
2-13-1b	2-13-63										
2-13-2a	2-13-63	63.9	4.62	18.1	35.6	14.9					
2-13-2b	2-13-63	63.9			35.6					Positive Power Perturbation	Flow oscillation just barely overshot the second time. The pressure data exhibits one overshoot before stabilizing out.
2-13-3a	2-13-63	68.6	4.76	17.2	48.4	12.2					
2-13-3b	2-13-63										
2-13-4a	2-13-63	65.5	3.84	20.6	55.1	12.4		VALVE ADJ. FOR V $0.8\ V_o$			
2-13-4b	2-13-63										
2-13-5a	2-13-63	62.9	2.56	31.2	69.0	12.7		VALVE ADJ. FOR V $0.5\ V_o$		Negative Power Perturbation	Flow responds as if it is virtually critically damped. The pressure data appears to be similar to the flow data.
2-13-5b											
3-5-2	3-5-63	41.0			27.5					Negative Power	Flow oscillation damped after 2 cycles; overshot twice and settled out on the beginning of the 3rd oscillation. Pressure drop showed a similar characteristic.

Even number runs and "b" series runs are transient power runs corresponding to the conditions immediately preceding.

The pressure drop reading across the test section has consistently shown an oscillation component in the frequency range of 20 - 25 cps. It was suspected that its origin was from other than hydraulic flow dynamics, although other experimenters have also noticed oscillations in the frequency range of 20 - 25 cps.[4] The transducer electronic system was found not to be the source of the oscillations. Other sources were investigated, such as condenser fan vibration, induced mechanical or hydraulic oscillation, or building vibrations transmitted to the transducer mounting or to the hydraulic system. Further examination of data indicates the possibility of oscillations in pressure drop due to two-phase flow mechanisms. It is shown that these are true pressure oscillations on runs where the scale factors for inlet and discharge pressures were sufficiently enlarged to show the oscillations also to be present in the static pressure signals.

The steady-state velocities obtained from the experiments and from the analytical model are shown in Figure 9. The loop conditions were:

1. Minimum external loop resistance,
2. Natural circulation, and
3. 1000 psi pressure.

The agreement is excellent above 10 percent quality, but as the quality decreases below 10 percent, the deviation increases to about 8 percent at quality of about 3 percent. For two-phase flow systems, this is good agreement.

In Figure 10, the recorded traces are shown for Run No. 1-31-6, which is a positive power impulse transient run. Some of the pressure traces have been overlapped for comparison purposes. The bottom trace shows the instantaneous test section current. The power is proportional to the square of the current and the increase and decrease of power are steeper than shown by the current trace. The power increase phase of the transient occurred in 0.30 seconds while the power decrease occurred in 0.6 seconds. The total length of the impulse is about 0.90 seconds.

From a power impulse transient test, the following information is obtained:

1. Damped oscillation frequency, from peak-to-peak time intervals.
2. Quadratic damping coefficient, from oscillation decay envelope.
3. Time lags (or phase) of pressure and velocity to power impulse. Information on pressure propagation is obtained.
4. Magnitude and character of pressure and velocity changes.

The conditions for the positive power impulse transient test shown in Figure 10 were:

1. Run No. 1-31-6,
2. Pressure 1000 psi,
3. Natural circulation, minimum loop resistance,
4. Power 78.1 KW (317 KW/liter of heater),
5. Velocity 4.79 ft/sec (7.97×10^5 lbs/hr-ft^2),
6. Inlet temperature, 491.3 F,
7. Subcooling, 63.9 Btu/lb, and
8. Exit quality, 17.8 percent.

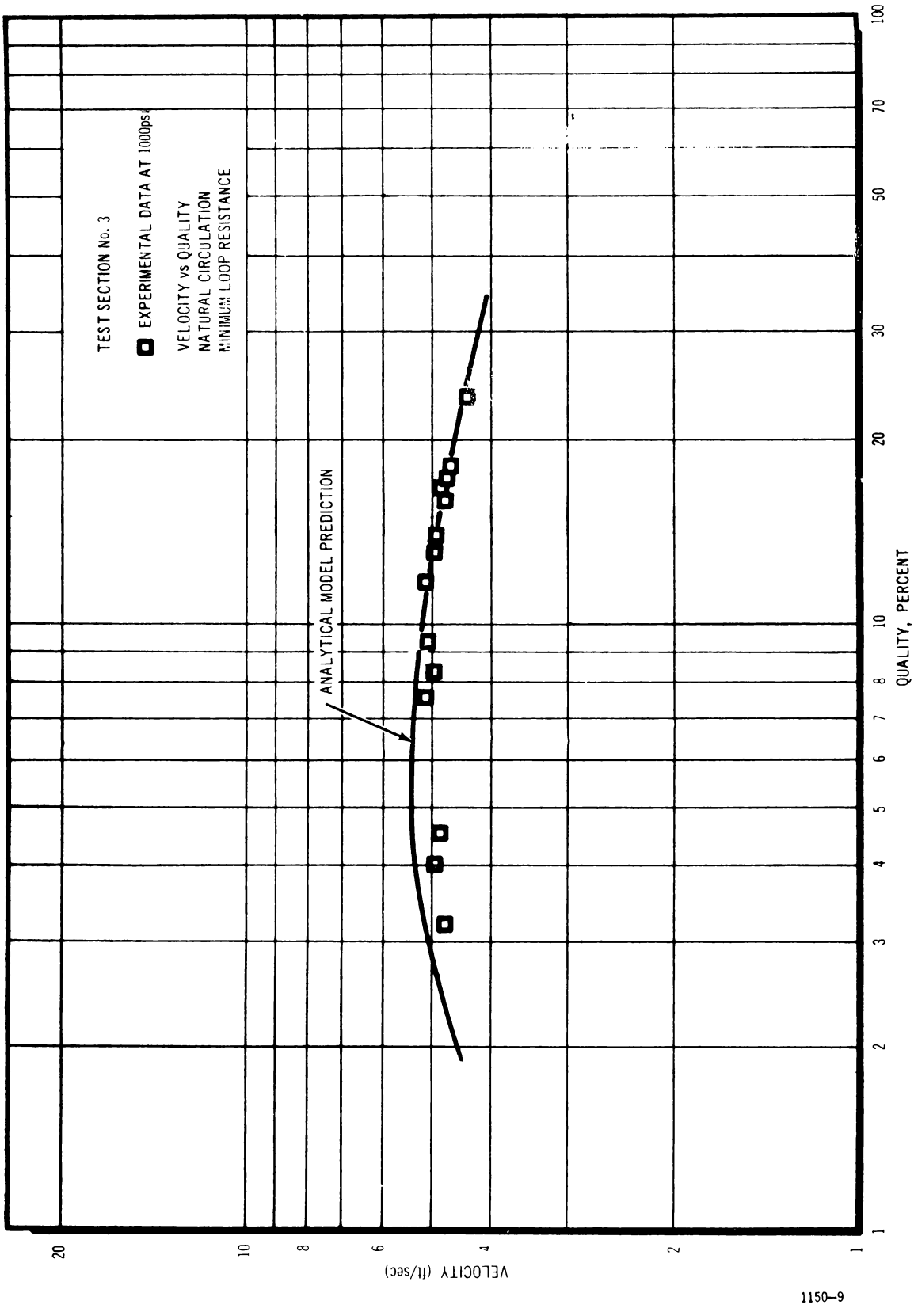

Figure 9. Comparison of Experimental and Analytical Velocities

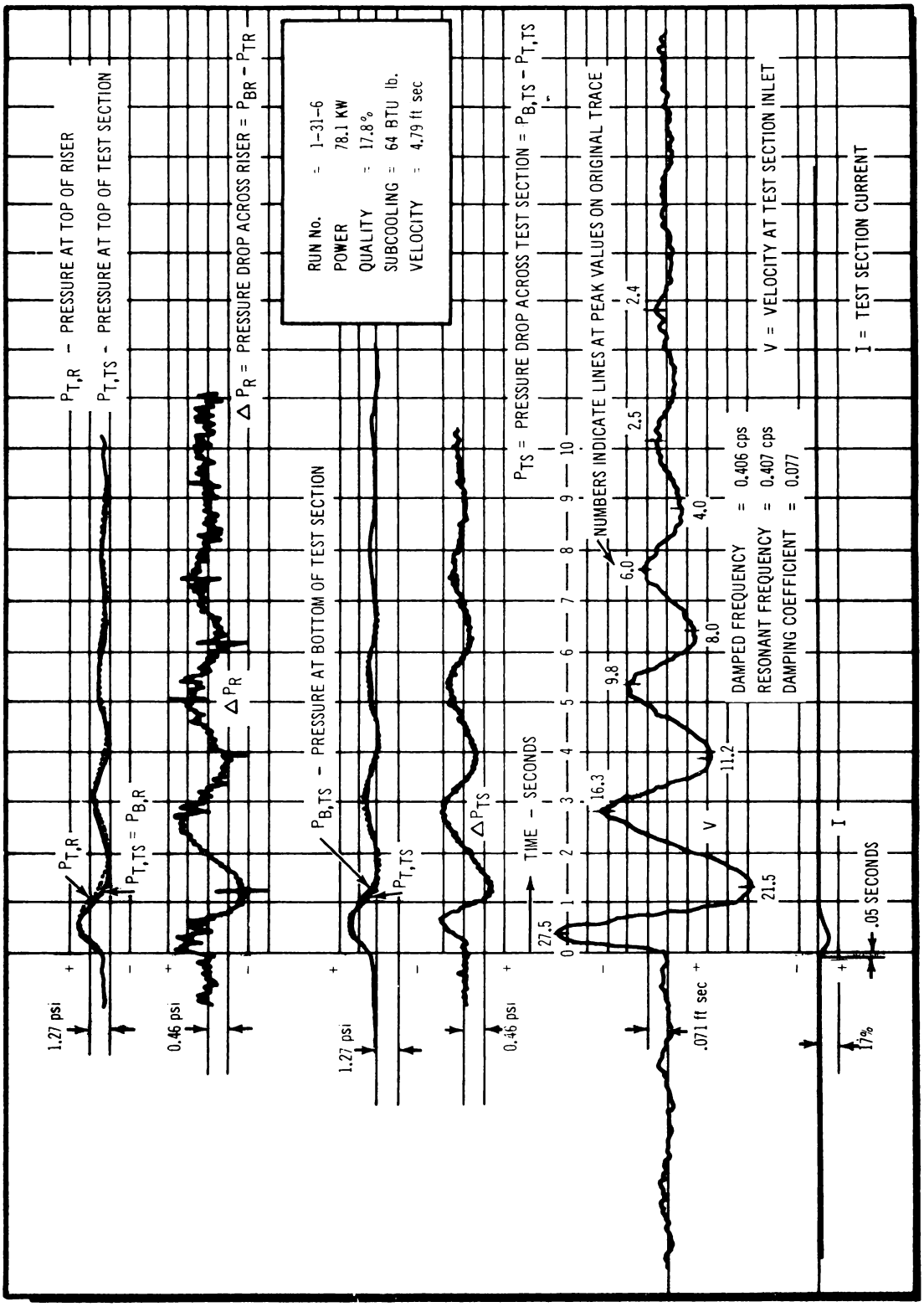

1150-10

Figure 10. Power Impulse Transient, Stability Loop Test

The damped oscillation frequency was 0.41 cps, and the quadratic damping coefficient was 0.077 (averaged value).

The response to the initial power increase of 19 percent was:

1. The inlet velocity decreased 8.2 percent. The time lag of the initial velocity response was 0.05 second.
2. The pressures at the top and bottom of the test section responded practically instantaneously (less than 0.020 second, which is the limit of detection from this trace). The two pressures rise almost identically for 0.30 second so that the pressure drop across the test section does not change until the power increase phase has been completed (0.30 second).
3. The pressure at the top of the riser has a 0.10 second time lag. This delay in pressure propagation to the top of the riser causes the riser pressure drop to increase immediately with the power impulse since the pressure at the bottom of the riser (top of test section) increases immediately with the power impulse. Therefore, the fluid in the riser would be expected to accelerate and increase its velocity during the power increase phase. No riser velocity measurements are available to confirm this. This is opposite to the trend for the inlet velocity to the test section. The time lag of 0.10 second corresponds to a velocity of pressure propagation of roughly 140 ft/sec. for the 13.75 foot long riser.

The response to the power decrease phase of the impulse transient is:

1. A 0.15 second delay before the velocity transient reaches its negative peak.
2. The power is practically back to the initial value in 0.8 second. At this time, the velocity has also returned to its initial value, but has a steep slope. The pressures, however, are about 1.5 psi above their initial values at this point.
3. The pressures reach their peak values about 0.35 second after the power peak.

These traces were obtained at a chart speed of 10 mm/sec. Other traces are available which were run at 50 mm/sec. Time lags and phase relationships obtained from these traces should be more precise.

The analytical model had been used for some pre-test analyses. The results of some of these analyses are given below:

Quality	Subcooling	Resonant Frequency cps	Quadratic Damping Coefficient	Reciprocal of Two-Phase Transit Time
4.3	20.5	0.272	0.110	0.362
8	38.1	0.414	0.110	0.486

Quality	Subcooling	Resonant Frequency cps	Quadratic Damping Coefficient	Reciprocal of Two-Phase Transit Time
16	76.3	0.268	1.0	0.676
32	152.5	0.083	1.0	1.007
4.3	12	0.257	0.93	0.350
8	12	0.339	0.161	0.453
16	12	0.457	0.120	0.599
32	12	0.666	0.048	0.855

Extrapolating the predicted results to 17.8 percent quality:

	Quality	Subcooling	Resonant Frequency cps	Quadratic Damping Coefficient	Reciprocal of Two-Phase Transit Time
Calculated	17.8	85	0.247	1.0	0.705
	17.8	12	0.481	0.112	0.622
Test	17.8	64	0.406	0.077	---

Although the test was conducted at a relatively high subcooling, the resonant frequency and damping coefficient are more typical of the results of the low subcooling analysis. This point will be further investigated. In addition, the analyses will be checked at other conditions to determine whether the tests continue to deviate from the predictions.

Further consideration of the run 1-13-6 indicates that an additional observation and tentative conclusion should be made. Data show that both the bottom and top pressures of the test section increase in almost identically the same manner for the first 0.30 second, during the rising power period. During this period, there was an increase in power by 19 percent with no increase in pressure drop across the heater channel, but an increase in heater section static pressure. This would not occur as the result of a two-phase flow phenomenon, but as the result of a wave propagation phenomenon. It has the effect of making the heater section a capacitance for this interval. The thermal responses would contain a transient under these circumstances. Presumably, such a phenomenon could be handled by a multi-node thermal hydraulics analysis. Further analysis of the data must be made to ascertain the character of the events taking place.

Two columns which have not been discussed are shown in Table VII. These are the last two columns on the right. One column summarizes the type of power perturbation introduced during steady-state operation for a number of key runs; the other column gives a qualitative description of the responses of the various measurements which are significant to characterizing stability responses.

Table VIII is a summary which for comparison purposes, demonstrates the damping of the flow

TABLE VIII

COMPARISON OF RESPONSES OF STABILITY LOOP

		High Power			
1)	64 - 67 KW	2-13-2b	Medium Subcooling	37 Btu/lb	Nearly critically damped
		1-29-8	Intermediate Subcooling	49 Btu/lb	Under-damped: Overshot twice
		2-13-5a	High Subcooling	69 Btu/lb	Nearly critically damped
		"Low" Subcooling			
2)	Δh_{sub} = 18 - 20 Btu/lb	1-29-2	Low Power	18 KW	Nearly critically damped
		1-29-10	Medium Power	29 KW	Nearly critically damped
		2-1-1b	Intermediate Power	37 KW	Overshot second time (small)
		2-13-2b	High Power	64 KW	Nearly critically damped
		"Medium" Subcooling			
3)	Δh_{sub} = 35 - 38 Btu/lb	2-13-2b	High Power	64 KW	Overshot second time (small)
		1-29-6	Intermediate Power	55 KW	Overshot twice

in natural circulation operation of the loop. The first grouping represents approximately constant power runs with varying subcooling. This indicates a surprising result in that the intermediate subcooling is apparently less damped than the higher subcooling. Further study of this will be required to determine the cause. When the low subcooling group is considered, again the intermediate values of the independent parameter (here it is power) show less damping than the higher power runs. In this set of runs, however, the quality of the last run is high, so that the two-phase pressure drop has increased sharply. It is logical that some degree of increase in damping could have occurred in this situation. Such an increase in the two-phase pressure drop is demonstrated in Figure 9. The medium subcooling runs demonstrate generally more under-damped conditions. A study of both data and the theoretical predictions will be required to evaluate the relationship between theory and experiment.

Development of the hydraulic stability loop test facility for future work is continuing. Work has progressed during this reporting period on the installation of power oscillator equipment, which will be ready for operation in a few weeks.

An X-ray void detection apparatus is also being studied for application to the loop in the near future. This equipment will allow a completely integrated set of transient two-phase measurements to be made, and is a significant step to resolution of two-phase hydraulic stability analysis.

VBWR Data Analysis Program

Continued work on the advanced model analysis program has shown that additional steps in analysis are required in order to properly evaluate the stability and transient response analytical model used for the pre-test analysis. The steps in the program include:

1. Recalculation of the analytical model predictions for the exact conditions of the experimental data. It is this stage which has been modified. The modification consists of an investigation to place the thermal hydraulic analyses contributing to void reactivity calculations, two-phase pressure loss and flow distribution calculations, and the stability and transient response analysis on a basis as nearly the same as possible. This step is being taken to improve the final analytical model evaluation.
2. The experimental data will be reduced, using the refined methods provided by the Boonshaft-Fuchs Spectrum Analyzer. This analyzer is now in a preliminary operating stage.
3. The analytical comparison of model prediction and experimental data will then be made.

Data of a portion of the runs considered most important in the VBWR stability tests have been re-recorded, using two Ampex FM tape recorders. The purpose of the re-run is to obtain shortened lengths of tape for analysis on a tape loop. This operation performs two improvements in data analysis. The first is that in re-recording; the tapes, originally recorded at 15 inches per second, are re-recorded at 1-7/8 inches per second. Playback of these tapes at 15 ips gives a step up in frequency of a factor of 8. This puts the important frequencies being examined in a

range which improves the frequency resolution of the Boonshaft-Fuchs analyzer. The second improvement comes from the fact that a tape loop mechanism can then be used. This allows continuous data scanning of the tape trace without the starting length error, although a spurious signal (which can be readily recognized) is put in at a frequency corresponding to the time for one circuit at the tape loop. This signal is due to joining the two ends of the tape to form the tape loop.

TASK B - HEAT TRANSFER AND FLUID DYNAMICS

The heat transfer task is being conducted to obtain design data on the critical heat flux, to gain understanding of the phenomena involved, and to raise the limit. Critical heat flux measurements have been completed for the single rod (annular), and rectangular geometries and measurements with a multirod geometry have been started. The previous work provides the basis for investigating methods of increasing the critical heat flux limit.

Results are reported for: (a) single-rod tests, (b) multi-rod tests, (c) methods for increasing the critical heat flux, and (d) effect of a bowed heater rod.

A comprehensive topical report on the single-rod burnout heat flux measurements during 1960, 1961, and 1962 has been prepared. The report, Burnout Conditions for Single Rod in Annular Geometry, Water at 600 to 1400 psia, by E. Janssen and J. A. Kervinen, GEAP-3899, February 1963, is summarized as follows:

"Tests were run at General Electric, APED, to determine burnout conditions for a rod in an annular geometry. An electrically heated rod was placed in a circular tube to form the annular flow path for the water coolant. Only the rod was heated, the outer surface (tube) being essentially adiabatic. Orientation was vertical, with flow up. The tests covered the following range of conditions (corresponding to conditions which might exist in a reactor core):

Rod O D :	0.375 to 0.875 inch
Tube I D :	0.555 to 1.250 inch
Hydraulic Dia.:	0.180 to 0.875 inch
Heated Length:	29 to 108 inches
Pressure:	600 to 1450 psia
Flow Rate:	0.14×10^6 to 6.2×10^6 lb/hr-ft^2
Steam Quality:	Slightly subcooled to 61.5 percent

"For each condition the electrical power was increased until burnout was reached, thus establishing a burnout condition for the particular rod and tube geometry.

"The basic test geometry was a straight concentric annulus. The burnout results for this geometry showed that:

1. When burnout heat flux is plotted versus quality (other variables held constant), the points (except for experimental scatter of the order of ±10 percent maximum) lie on a straight line. The line slopes downward in the direction of increasing quality.
2. An increase in flow (other variables constant) results in a decrease in burnout heat flux for flows up to about 2×10^6 lb/hr-ft^2.
3. An increase in the hydraulic diameter (other variables constant) from 0.18 inch to 0.25 inch results in an increase in the burnout heat flux. For an increase from about 0.25 inch to 0.5 inch, the burnout heat flux goes through a maximum. An increase from 0.5 inch to 0.875 inch results in a decrease in the burnout heat flux.

4. An increase in pressure (other variables constant) results in a decrease in burnout heat flux, for pressures in the range 600 to 1450 psia.

"Of the basic test geometry data which fall within the following range of conditions,

Hydraulic dia.:	0.25 to 0.875 inch
Pressure:	600 to 1450 psia
Flow:	0.14×10^6 to 6.2×10^6 lb/hr-ft^2
Quality:	-0.12 to 0.45
Heat Flux:	$\emptyset_{bo} > 0.35 \times 10^6$ Btu/hr-ft^2

95 percent are correlated to ±20 percent by

$$\frac{\emptyset_{bo(c)}}{10^6} = \frac{\left[1 + 0.16\left(\frac{1000-P}{400}\right) - 0.04\left(\frac{1000-P}{400}\right)^2\right]}{1-0.008\,B\left(\frac{G}{10^6}\right)^{0.8}}\left[0.0172\,B\left(\frac{G}{10^6}\right)^{0.8} - \left\{0.3175\left(\frac{G}{10^6}\right)^{-2} - 1.8534\left(\frac{G}{10^6}\right)^{-1}\right\} - \left\{2.4 + 3.2\,D_h + 0.83 D_h\left(\frac{G}{10^6}\right)\right\}\right\} \times$$

$$\left\{-0.0629\left(\frac{G}{10^6}\right)^{-2} + 0.3429\left(\frac{G}{10^6}\right)^{-1} - 0.2494 + 0.0020\left(\frac{G}{10^6}\right)^2\right\}\Bigg]$$

"The above range of conditions marks the limits of validity for this correlation.

"Certain modifications of the basic test geometry were also tested. These are:

1. Eccentric rod
2. Simulated spacer
3. Sandblasted rod

(Special geometries)

4. Rough Liner (0.875 inch ID tube fitted with 0.70 inch ID × 0.080 inch rings on 1 inch centers)

"The burnout results for these geometries show that:

1. When the rod is moved to 0.033 inch from the wall, the burnout heat heat flux may be reduced by from 22 percent to 50 percent.
2. The burnout heat flux remains unchanged when the flow is forced to separate from the heated surface (simulating flow just ahead of a plate-type spacer).
3. When the rod surface is roughened to 300 microinches, such as by sandblasting,

the burnout heat flux may be reduced by 35 to 50 percent.

4. Burnout heat flux for the rough liner is greater than for the smooth liner (i.e., basic test geometry), by about 40 percent at a flow of 0.56×10^6 lb/hr-ft^2, 20 percent at 1.12×10^6 lb/hr-ft^2. The slope of the burnout heat flux vs. quality curve through the data points is less for the rough liner at 1.12×10^6 lb/hr-ft^2 than for the smooth. The rough liner results show little or no flow effect.

"The basic test geometry data are compared with other internally heated annular data, from Columbia University, Italy, and Great Britain. Direct comparison cannot be made with the Italian results; agreement with the Columbia results is good, and with the British results, poor. Poor agreement with the British is attributed to the difference in conditions at the APED test section inlet (subcooled liquid) as compared with conditions at the British test section inlet (two-phase).

"The basic test geometry data are compared with multirod data now available from Columbia, Hanford, and General Electric, APED. The slope of the heat flux vs. quality curve for the multirod data is generally less than the corresponding curve for the single rod data (although the Columbia multirod data do not show this). There is little or no flow effect for the multirod. The differences between single and multirod results are attributed to flow disturbances in the multirod test sections. These flow disturbances are caused by the provision for maintaining spacing between adjacent rods, made necessary by the strong electromagnetic forces acting between parallel conductors. The cleanest multirod flow channel (Columbia 7-rod, non-wrapped) gave results which are in good agreement with the single rod results."

Multi-rod Tests

The four-rod test section was assembled and shake-down operation in the heat transfer loop was conducted during January. Initial difficulty with cooling of the flexible electrical leads at the top of the heated rods, and with dimensional tolerances between the test section and housing pipe have been corrected. The four-rod test section has been operating successfully since the beginning of February. To date, 17 burnout data points have been obtained, 3 of them actual rod failures. The data has been obtained at 1000 psia and at mass velocities of 0.5, 1.0 and 1.5 lb/hr-ft^2, at qualities of 10 to 25 percent.

The data thus far generally agree with the single-rod results reported above (GEAP-3899) with the critical heat flux values being slightly higher in the four-rod geometry.

The location of the three rod failures ("burnout") which have occurred is, of itself, a significant result. Each of the failures occurred at the exit end and at a point on the rod which faces the corner of the channel. This result is in agreement with previous observations and tends to confirm the significance of the liquid film on the adjacent unheated channel wall, as discussed below. The corner fuel rod in a reactor fuel assembly is subjected to more severe conditions than the other rods in the fuel assembly because of: (1) neutron flux peaking at the edge of the fuel bundle, and (2) reduction in critical heat flux resulting from the liquid film on the adjacent channel wall.

Methods for Increasing the Critical Heat Flux

The evaluation of methods for increasing the critical heat flux is being reported in the topical report: Methods for Improving the Critical Heat Flux for BWR's, C. L. Howard, GEAP-4203, March, 1963. The report includes an evaluation of "film trippers" on the unheated channel walls. This concept has considerable promise, as presented below.

Consideration of the mechanisms postulated as controlling the critical heat flux phenomena leads quickly to the conclusion that any liquid flowing on the unheated channel wall is of no help in cooling the fuel rods. The film on the unheated surface is parasitic in that it robs the heated surface of liquid which would otherwise be available. This conclusion is substantiated by comparison of critical heat flux data for various test section geometries having different ratios of heated to unheated surface. The critical heat flux is decreased as the fraction of the heated surface is decreased in the following list:

1. All surfaces heated:

   Flow inside round tubes
   Flow in an annulus heated both internally and externally

2. Over half of surfaces heated:

   Rectangular channel heated on the two long sides

3. Less than half of surfaces heated:

   Flow in an annulus heated internally.

A typical multirod reactor fuel bundle has over half its surface heated since the perimeter of the fuel rods is greater than the perimeter of the channel. Then which test section geometry is applicable to the reactor fuel bundle? Since the heat flux is limited by the corner rods, the cautious approach is used.[5] The outer quarter of the perimeter of the corner rods is considered analogous to flow in an annulus heated internally. The test data for annular geometry are then interpreted as being applicable to the reactor fuel bundle. Multi-rod data being obtained in this program will indicate the extent to which this is valid.

If the detrimental effect of the liquid film on the unheated wall of the annular geometry can be prevented, this would be of direct significance to the reactor design limits.

One method of removing the liquid film from the unheated wall has been given preliminary tests. The discussion and results which follow are based on the work of E. Janssen and J. A. Kervinen conducted in March 1961 [6] and in March 1962 [7]. "Film trippers" were placed at intervals on the unheated wall of the single-rod (annular) test section. The film trippers were ridges (rings) extending 0.080 inch into the flow stream and 0.080 inch thick. This was also referred to as the "rough liner" test.

The theory of operation is that the liquid film flowing on the surface flows over the projecting ridge and at the crest of the ridge is sheared off and dispersed by the flow stream. This liquid

is then available to diffuse to the heated surface. Some of the liquid doubtlessly gets back to the unheated surface also. It is then removed by the next tripper. The first series of tests used a 1.0 inch spacing between trippers. In the second series of tests (March, 1962), the spacing between film trippers could be changed by adding spacer rings to give spacings of 0.50, 0.92, and 2.60 inches.

Several conclusions can be reached from this data:

1. At low steam qualities (Xe < 0.05) the film trippers show no advantage. This may indicate only that the theoretical model on which the film tripper concept is based is not applicable at low qualities.

   The critical heat flux in this region is over 1.15×10^6 Btu/hr-ft^2 which is high enough so that further increase is not needed as greatly as at higher quality.

2. The slope of the critical heat flux versus quality curve is decreased by the film trippers. This suggests that the limiting mechanism in the process has been changed. The slope appears to depend on the amount of surface available for flow of a liquid film on the unheated surface:

Geometry	Fraction of Perimeter Heated	Fraction of Perimeter with Parasitic Film	Flow lb/hr-ft^2	Slope q_c/X_e
Annular	0.30	0.70	0.5	-4.3
			1.13	-4.4
			1.68	-4.7
Rectangular	0.89	0.11	1.44	-2.0
Annular, with film trippers	0.30	0	0.5	-1.0
			1.1	-1.6

3. At high steam qualities (X_e > 8 to 16 percent depending on mass flow rate) the film trippers result in a distinct improvement in critical heat flux. As quality and flow are increased, the improvement becomes greater:

Quality	Flow	Improvement in Critical Heat Flux
15%	0.5×10^6 lb/hr-ft^2	None
15%	1.7×10^6 lb/hr-ft^2	48%
25%	0.5×10^6 lb/hr-ft^2	75%
25%	1.7×10^6 lb/hr-ft^2	>100%

4. The film trippers greatly reduce the detrimental effect of high mass flow rate on critical heat flux. This makes the trippers particularly advantageous for high-flow and high-quality systems.

5. The optimum spacing between film trippers is not certain from this data. The following conclusions are tentative:

   a. A spacing of 0.9 to 2.6 inches is generally better than 0.5 inch.
   b. Consideration of pressure drop and pumping power leads to interest in the larger spacing intervals.
   c. The data for all spacings tested fall in a band of ±15 percent for qualities above 5 percent. Therefore, the spacing does not appear to be critical in the range tested.

These first trials with film trippers on the unheated channel wall demonstrate the potential value of the concept. Testing of these devices in the multirod geometry is planned. It is necessary to determine whether a significant benefit is obtained from trippers in a multi-rod geometry or whether the relatively decreased unheated surface of a multirod geometry has already led to the improvement which results from reduction of the parasitic flow of water on the unheated surface.

Effect of a Bowed Heater Rod

The previous work [6] on the effects of reduction of the clearance between the fuel rod and the channel wall has been extended to the case of zero clearance. The tests were conducted in the single-rod test section with the heater rod bowed so that it touched the channel 5 inches below the exit of the 73-inch heated length. This condition approximates that which would be expected if the corner fuel rod were to bow sufficiently to make contact with the corner of the channel.

The object of the tests was to determine whether bowing of the heated rod to the point of making contact with the channel would cause a substantial reduction of the critical heat flux, in comparison with critical heat fluxes previously established for normal rod-to-channel clearances.

A total of 20 valid critical heat flux or "burnout" determinations were made, together with measurements of the heated surface temperatures during operation above the critical heat flux level. The data were obtained at 1000 psia and mass flow rates of 311 and 160 lb/sec-ft^2. These measurements have resulted in the following conclusions:

1. Bowing of the heater rod to the point of making contact with the test section liner, in simulation of possible corner fuel rod conditions, results in decrease of the critical or "burnout" heat flux level by as much as a factor of two, or more, at flow and steam quality conditions typical of power reactors.
2. Heated surface temperatures, after onset of the critical heat flux condition are of the order of magnitude of 1000 F, or more, depending on how high above the critical level the heat flux is, for heat fluxes of about 500,000 to 600,000 Btu/hr-ft^2.

The substantial reduction of critical heat flux level experienced is probably due to a combination of two underlying causes: (1) continuation of the trend observed in some of the older critical heat flux data of decreasing critical heat flux with decreasing effective hydraulic diameter (in the range of small hydraulic diameters) [8] and with decreasing heated surface-to-channel clearance;[9] and (2) flow blockage in the vicinity of contact between the heated rod and the liner

with resulting excessive rise of local steam quality. It is expected that the bowed rod data is a member of a family having as two governing parameters the heated surface-to-channel clearance in one case and the configuration of the bow (radius of bend) in the other case. The critical heat flux would be expected to rise as the clearance between heated surface and channel is made larger (for clearances of the approximate order of less than 0.060 inch).[8, 9] Conversely, as the radius of bend of the bow is made larger, with contact between the heated surface and the channel, the critical heat flux would be expected to reduce. The effect of these two parameters, clearance in the first case and bend radius in the other case, were not investigated in these tests. Thus, it remains possible that if a reactor were to have bowed corner fuel rods in contact with the channel with larger radii of bend than was used in the present tests, the corresponding critical heat flux levels could be substantially less than those shown here.

It is reasonable to speculate that the point of contact between the heated rod and channel is probably surrounded by a tiny area on the heated surface which is in contact with vapor (rather than liquid) at heat fluxes much less than the critical heat flux, due to the very restricted flow conditions in the vicinity of the point of contact. This tiny dry area might be of the order of approximately 0.1 inch in size. Under these conditions the heat transfer mechanism would be expected to be principally heat conduction in the heated rod material (or in the clad, in the case of reactor fuel) from the higher temperature dry spot to the immediately adjacent liquid-film covered parts of the heated surface where nucleate boiling would still be in process. Analogous to the behavior of the phenomenon as observed for relatively smooth channels without irregularities, [8] the critical heat flux condition is expected to manifest itself as an abrupt drying out of the liquid film over larger areas of the heated surface near the contact point, resulting in abrupt rise and fluctuations of the surface temperature in these regions. Although lack of precision in the experiment prevented accurate positioning of thermocouples beneath the contact point, the temperature measurements made at adjacent locations tend to support these speculations of the detailed mechanisms involved. As indicated in Table X, onset of the critical heat flux condition often occurred first 2 to 5 inches downstream from the original point of contact between the heater rod and the liner, probably due to a wake effect after the contact point coupled with the increase in steam quality in the downstream direction.

The test conditions employed are summarized in Table IX, and details of the test section, including the geometry of the bowed rod and the location of the thermocouples (TC) are given in Figures 11 and 12. The point of contact between the heated rod and the channel liner was nominally located about 5 inches from the exit end of the heated section. The bow in the rod was made approximately symmetrical and extended over a distance of about 12 to 15 inches upstream and downstream from the contact point. In the vicinity of the bow the liner was electrically insulated by means of a steel sleeve backed with "durabla" to prevent electrical shorting at the contact point. Voltage measurements on the insulated liner sleeve were made continuously throughout the experiment to verify for each run that the heater was actually in contact with the insulated liner sleeve.

The critical heat flux condition was defined for the purpose of taking data as the condition at

TABLE IX

BOWED ROD. NOMINAL TEST CONDITIONS

Pressure	1000 psi	
Flow Geometry	Single-Rod in Annulus (Figure 11. 12)	
Heater Rod. OD	0. 540 inch	
Liner. ID	0. 875 inch	
Concentric Annulus Thickness	0. 168 inch	
Length of Bow	24 - 30 inches	
Heated Length	73 inches	
Distance of Contact from End of Heated Section	5 inches	
Mass Velocity. lbs/sec-ft^2	311	160
Steam Quality Range	0. 047-0. 147	0. 168-0. 233
Number of Valid Critical Heat Flux or "Burnout" Determinations	16	4

TABLE X

BOWED ROD, CRITICAL HEAT FLUX AND "BURNOUT" DATA

Run No.	Type*	Date	P psia	G lbs/sec-ft^2	q_c 10^6 Btu/hr-ft^2	X	Remarks
1	SS	1-4-63	992	318	0.338	0.091	
2	SS	1-4-63	1000	318	0.362	0.100	
3	C	1-4-63	1000	319	0.452	0.139	q_c at Pos. #1
4	C	1-4-63	960	320	0.435	0.134	q_c at Pos. #1
5	C	1-4-63	945	320	0.435	0.132	q_c at Pos. #1
6	C	1-4-63	925	319	0.417	0.127	q_c at Pos. #1
7	BO	1-4-63	925	319	0.398	0.119	q_c at Pos. #1-5
8	SS	1-5-63	1000	318	0.365	0.100	
9	C	1-5-63	1005	318	0.460	0.145	q_c at Pos. #3
10	C	1-5-63	1015	318	0.476	0.147	q_c at Pos. #3
11	SS	1-5-63	1000	318	0.540	0.093	
12	SS	1-8-63	1000	318	0.492	0.067	
13-A	C	1-8-63	1001	318	0.587	0.112	q_c at Pos. #3
14-A	C-R	1-8-63	915	311	---	---	Conditions Uncertain
15-A	C-R	1-8-63	915	311	---	---	Conditions Uncertain
16-A	BO-R	1-8-63	915	313	0.603	0.193	(q_c at Pos. #5) Cond. Uncertain
13	SS	1-8-63	1000	318	0.365	0.104	
14	C	1-8-63	1000	319	0.444	0.138	
15	SS	1-8-63	983	319	0.508	0.065	
16	C	1-8-63	1000	319	0.524	0.077	
17	C	1-8-63	995	319	0.524	0.068	
18-1	SS	1-9-63	955	318	0.556	0.060	
18-2	C	1-9-63	955	318	0.571	0.059	
19-1	SS	1-9-63	955	160	0.302	0.168	
19-2	C	1-9-63	1005	160	0.381	0.229	
20	SS	1-9-63	1000	160	0.333	0.190	
21	C	1-9-63	1013	160	0.381	0.233	
22	C	1-9-63	990	161	0.414	0.224	
23	C	1-9-63	1000	318	0.540	0.076	q_c at Pos. #1
24	SS	1-9-63	972	318	0.603	0.068	
25	C	1-9-63	987	318	0.603	0.067	q_c at Pos. #1
26	C	1-9-63	945	161	0.317	0.185	
27	C	1-9-63	1020	318	0.517	0.098	q_c at Pos. #1
28-1	C	1-9-63	990	321	0.524	0.047	q_c at Pos. #1
28-9	BO	1-9-63	1025	315	0.659	0.112	q_c at Pos. #1-5

*SS - Steady-state run

C - Valid critical heat flux data

BO - Heater element failed (valid)

-R - Invalid run (rejected)

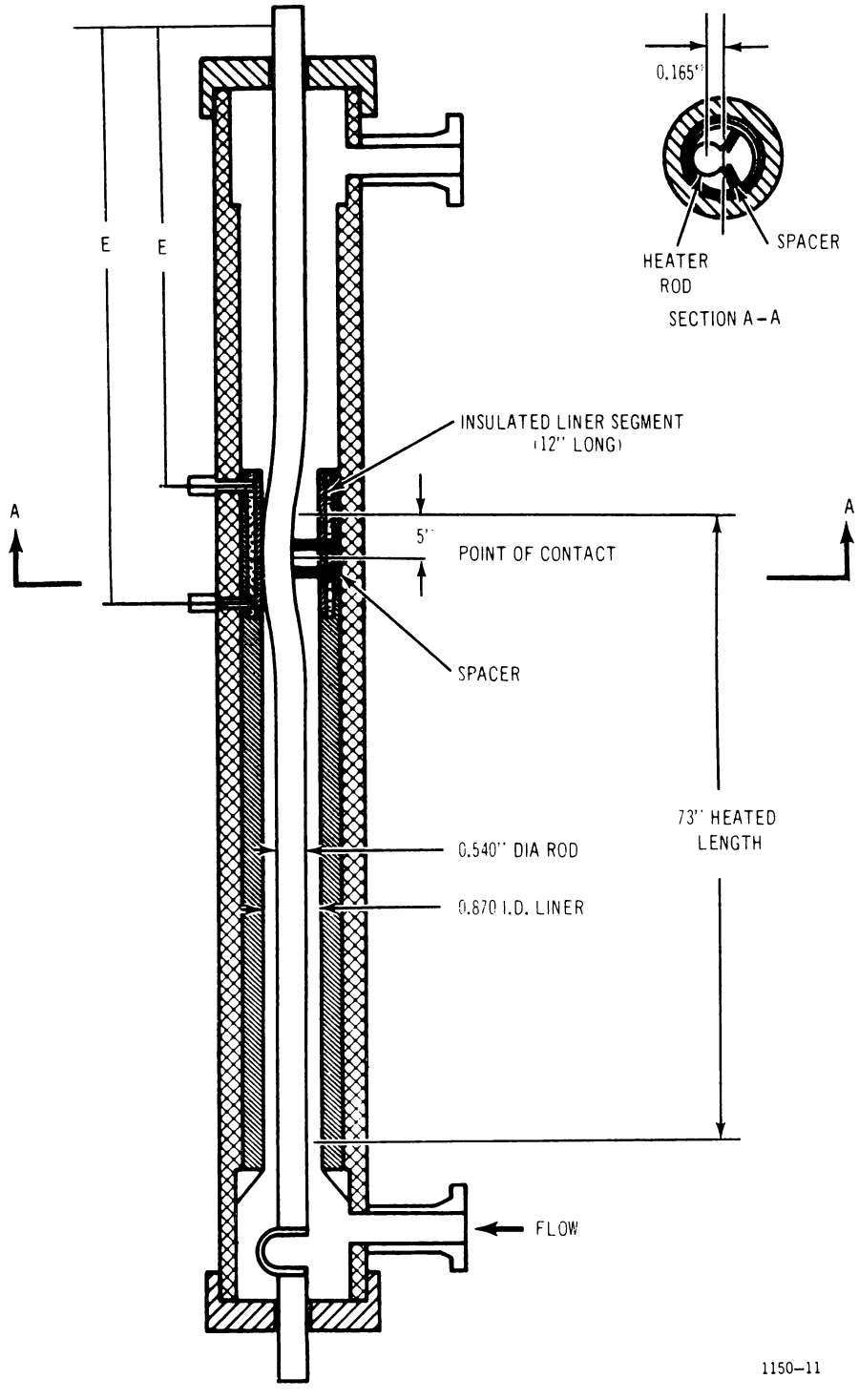

Figure 11. Single Rod Burnout Bowed Rod

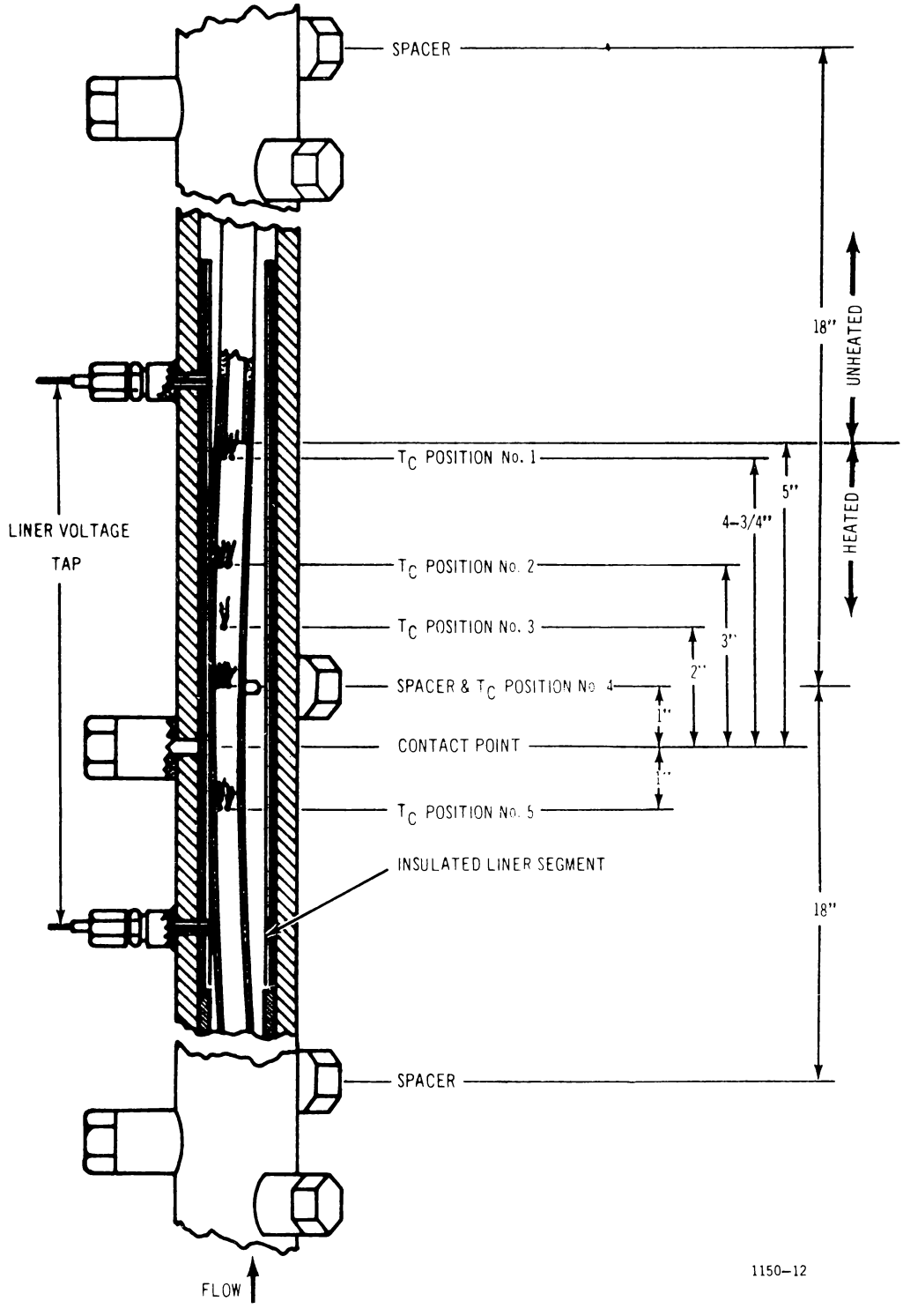

Figure 12. Detail of Bowed Rod

which abrupt rise or commencement of substantial oscillation of the heated rod surface temperature occurred, as indicated by either the recorded output from thermocouples attached to the heated wall or the character of the output signal from a resistance bridge circuit (detector) connected across two 9-inch tapped sections in the last 18 inches of the heater rod. For each run the critical heat flux condition was approached by slowly raising the heat flux in small increments while the flow, pressure and inlet subcooling were held constant.

A total of sixteen valid critical heat flux or "burnout" determinations were made at a nominal mass velocity of 311 lbs/sec-ft^2, plus four determinations at a mass velocity of 160 lbs/sec-ft^2. These data are given in Table X, and the 311 lbs/sec-ft^2 mass velocity data is plotted in Figure 13. It is shown by Figure 13, for the 311 lbs/sec-ft^2 mass velocity data, that the critical heat flux for the bowed rod lies substantially below both the APED design burnout limit currently in design usage [5] and the data obtained earlier for a concentric annulus at comparable operating conditions. [6] A similar trend is exhibited by the four data points taken at 160 lbs/sec-ft^2 mass velocity (not plotted). The reduction of the critical heat flux for the bowed rod is as much as a factor of two or more in some areas of low steam quality operation (Figure 13).

Heated surface temperatures and corresponding average heat transfer convection coefficients are listed in Table XI as measured during continued operation to heat fluxes above the critical heat flux level into the "transition boiling regime" (final run No. 28). The temperatures were measured at the positions indicated, on the side of the heater rod in contact with the insulated liner. At onset of the critical heat flux condition (run No. 28-1 in Table XI) the surface temperature at the end of the heated section, 4-3/4 inches downstream from the point of rod-to-liner contact, commenced to oscillate slightly with an amplitude of about 40 F and a peak surface temperature of 689 F. Further increases in the heat flux (and steam quality) caused substantial increase in the peak temperature at this location and some increase in the oscillation amplitude. At about 125 percent of the critical heat flux (run No. 28-8 in Table XI) the surface temperatures at the other thermocouple locations, in the vicinity of the contact point, rose abruptly, the one closest to the contact point (position 4) becoming about 1300 F with slight oscillation. The last heat flux increase (run No. 28-9) resulted in failure of the heated rod due to short circuiting upstream from the insulated liner section. At the instant of failure the surface temperatures were all rising and ranged from about 900 F to as high as about 1980 F at the positions indicated. The progress of run No. 28 from inception of the critical heat flux condition (run No. 28-1) to failure of the heater rod (run No. 28-9) is graphed in Figure 13 as a dashed line with arrow connecting the beginning and terminal points. During this run the effective average convection heat transfer coefficient, h, deteriorated from about 4,000 Btu/hr-ft^2-°F at the beginning of the run to about 450 Btu/hr-ft^2-°F for position 1 at the end of the heated section, and decreased from about 900 to about 650 Btu/hr-ft^2-°F for position 4 near the point of contact, after critical heat flux conditions had occurred. The duration of the run was about 25 minutes, during which the heat flux was raised to about 26 percent above the initial critical level.

The heater rod used in run No. 28 has extensive "dimpling" both at near the contact point and at the downstream end, resulting from the 1000-psi external pressure acting in conjunction with

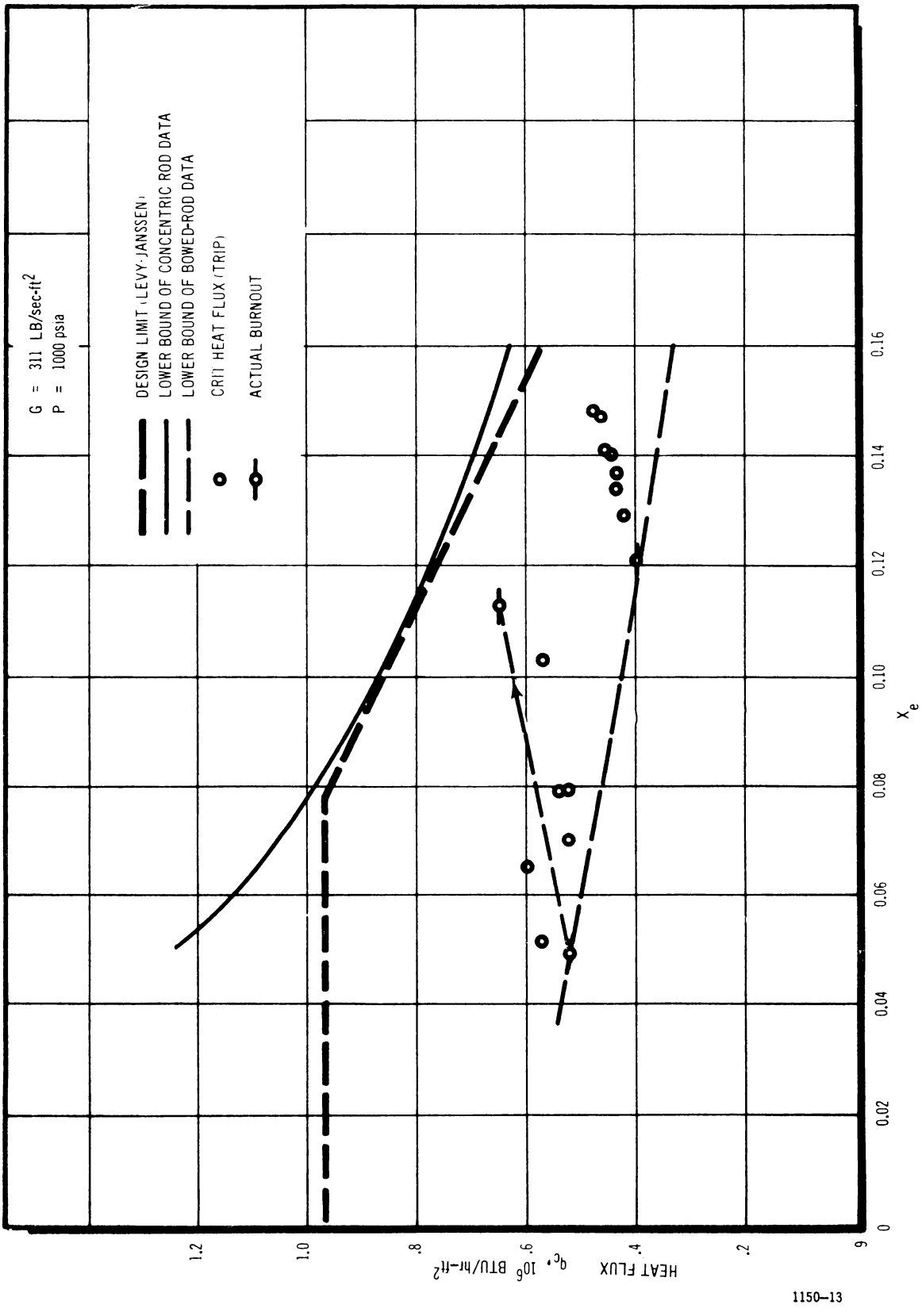

Figure 13. Critical Heat Flux and "Burnout" with Bowed Rod

TABLE XI

SURFACE TEMPERATURES AND MEAN HEAT TRANSFER

COEFFICIENT DURING OPERATION ABOVE CRITICAL HEAT FLUX

Run No.	P psia	G lb/sec-ft^2	X	q 10^6 Btu/hr-ft^2	Surf. Temp., °F $\frac{\text{max.}}{\text{min.}}$				Mean Coeff., Btu/hr-ft^2-°F			
					Pos. -1**	Pos. -2	Pos. -3	Pos. -4	Pos. -1	Pos. -2	Pos. -3	Pos. -4
28-1	990	321	0.047	0.524	$\frac{689}{650}$				4140			
28-2	↓	↓	↓	0.548	$\frac{913}{731}$				1970			
28-3				0.556	$\frac{1063}{996}$				1148			
28-4				0.571	$\frac{1130}{1036}$				1060			
28-5				0.595	$\frac{1150}{1107}$				1020			
28-6				0.611	$\frac{1272}{1229}$				869			
28-7				0.635	$\frac{1386}{1302}$				794			
28-8				0.651	$\frac{1780}{1678}$	1148	661	$\frac{1298}{1277}$	550	1081	5700	878
28-9	1025	315	0.112	0.659	1983*	1451*	909*	1550*	458	730	1821	658

* - Run terminated due to heater rod failure; temperature rising.

** - Positions of temperature measurement located as shown in Figure 12.

softening of the metal at the high local temperature experienced during the run to heat fluxes above the critical level. It is possible that the dimpling may have occurred early during run No. 28 and, hence, further prevented coolant flow to the dimpled surface, thereby causing the excessively high local temperature measured at the end of the run (1980 F).

On this rod and on the two others that failed (due to pinholes caused by short-circuiting) during earlier test runs there can be seen relatively large zones where the metal is blackened, due to the high temperatures experienced during momentary operation above the critical heat flux level. On two of these rods the zones of high temperature are located both slightly upstream of the point of contact and at near the end of heating four to five inches downstream. They are each shaped like an oval about one and a half to two inches long and a half inch wide, on the side of the rod closest to the channel (rods failed during runs 7 and 28-9). On the other rod the high temperature zone extends from the contact point to about an inch upstream, also on the side of the rod closest to the liner. The material used for all of the heater rods was seamless stainless steel tubing, Type 304, with 0.049 inch wall thickness.

TASK C - EXPERIMENTAL PHYSICS

The long term reactivity and nuclear physics characteristics of the fuel are being investigated by isotopic analysis of uranium and plutonium content of irradiated fuel. Irradiation of Task C elements 17J and 18J continues. The accumulated exposure for the elements is about 3200 MWD/T (average).

Experimental determination of burnup and isotopic composition has been completed on six radial samples. These samples are taken from pellet 9 (about 6 inches from bottom of rod) of rod R2H2. R2H2 had an average exposure of 1000 MWD/T. The samples were obtained by drilling into the end of the fuel pellet at various positions along one diameter with 60 and 30 mil burr drills. The fuel dust from the drillings was collected on filter paper, then dissolved and analyzed. Results of this analysis are shown in Table XII. Data from a sample taken at the center of the pellet will be available at the next reporting period. The exposure shown here is that obtained from Ce-144. Because of the large decay correction, the Zr-95 data are good only in a relative sense. The Cs-137 data are about 20 - 25 percent higher than that from Ce-144. This is possibly due to migration toward the periphery. The Ce-144 data are in good agreement with previously reported data on the adjacent pellet 10.

Figure 14 shows the Pu-239, 240, and 241 atom concentration as a function of pellet radius. When data are available on the center sample, a more detailed interpretation of this measured data will be reported.

TABLE XII

RADIAL VARIATION IN ISOTOPIC COMPOSITION

Sample Locations (mils)	Drill Size (mils)	Uranium Isotopic Composition (Atom %)			
		U-234	U-235	U-236	U-238
0-8*	60	0.012 ± 0.001	2.571 ± 0.008	0.049 ± 0.003	97.367
8-13	30	0.014 ± 0.001	2.635 ± 0.005	0.052 ± 0.001	97.299
13-18	30	0.015 ± 0.002	2.61 ± 0.01	0.051 ± 0.001	97.32
18-23	30	0.015 ± 0.001	2.551 ± 0.006	0.052 ± 0.002	97.382
43-73	30	----	2.54 ± 0.01	0.047 ± 0.008	97.40
0-19**	30	0.018 ± 0.001	2.657 ± 0.01	0.0533± 0.001	97.282

PLUTONIUM ISOTOPIC COMPOSITION (ATOM %)

Sample Locations (mils)	Plutonium Isotopic Composition (Atom %)			$(\frac{\text{Pu-239}}{\text{U-238}}) \times 10^3$	MWD/T
	Pu-239	Pu-240	Pu-241		
0-8	96.496	3.31 ± 0.01	0.190 ± 0.003	1.50 ± 5%	1300 ± 90
8-13	96.61	3.20 ± 0.02	0.187 ± 0.006	1.19 ± 5%	1360 ± 100
13-18	96.63	3.18 ± 0.01	0.174 ± 0.001	0.84 ± 5%	1340 ± 90
18-23	96.702	3.124 ± 0.004	0.174 ± 0.003	0.63 ± 5%	1250 ± 90
43-73	96.68	3.17 ± 0.01	0.15 ± 0.05	0.59 ± 5%	1250 ± 90
0-19	96.72	3.11 ± 0.03	0.169 ± 0.003	1.02 ± 5%	1310 ± 90

* 0 mils indicates inner edge of clad.

**(Opposite Side of Pellet)

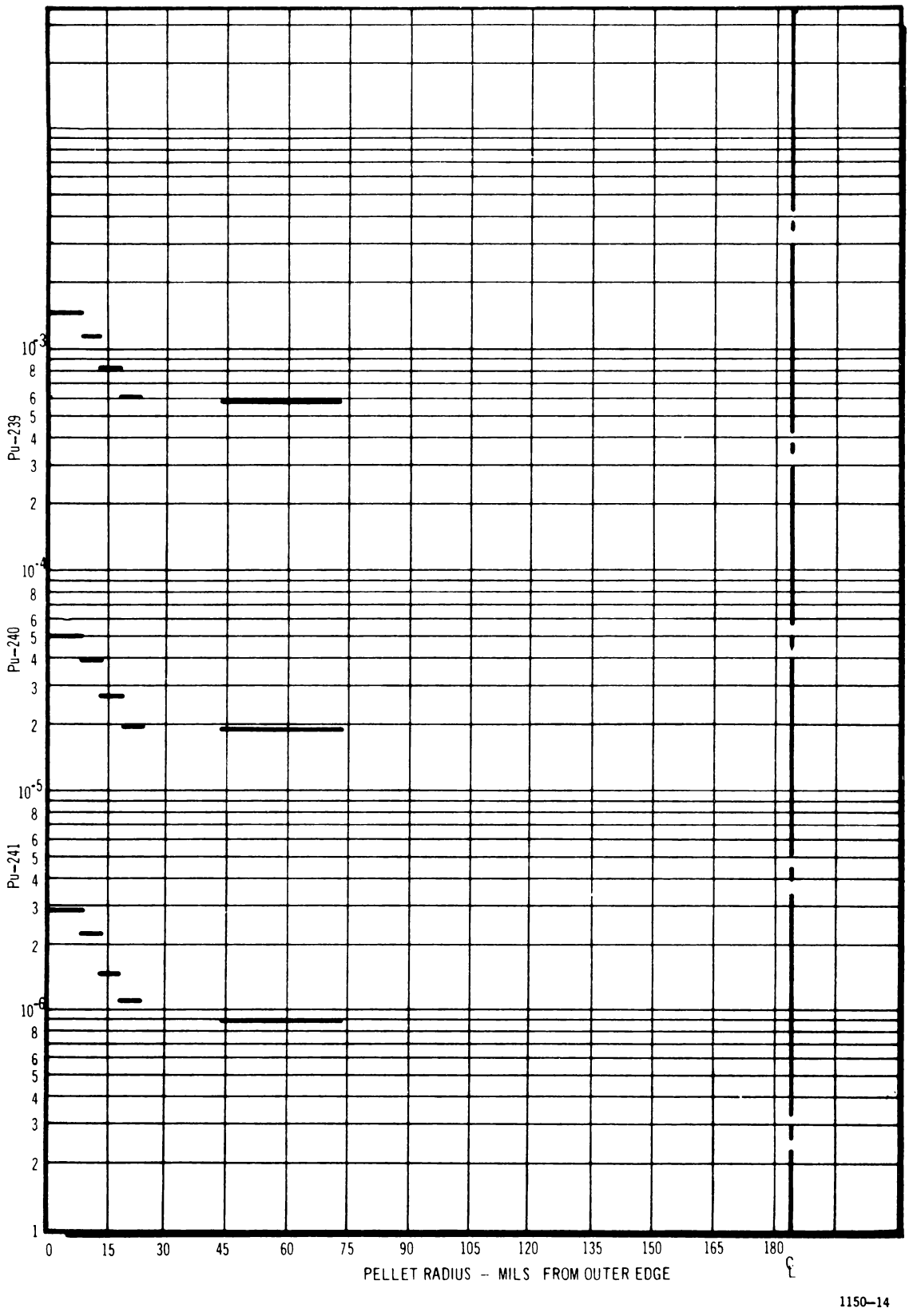

Figure 14. Radial Variation in Plutonium Atom Fractions in Fuel Pellet

REFERENCES

(1) R. L. Holladay, High Power Density Development Project, Tenth Quarterly Progress Report, July - September, 1962, GEAP-4094.

(2) R. L. Holladay, High Power Density Development Project, Eleventh Quarterly Progress Report, October - December, 1962, GEAP-4155.

(3) R. L. Holladay, High Power Density Development Project, Twelfth Quarterly Progress Report, January - March, 1963, GEAP-4219.

(4) Report EURAEC-313, Technische Hogeschool, Eindhoven, The Netherlands.

(5) Janssen E. and Levy S., Burnout Limit Curves for Boiling Water Reactors, APED-3892, April 1, 1962.

(6) GEAP-3899, summarized on pages 35-37.

(7) Unpublished data.

(8) GEAP-3766, Critical Heat Flux and Flow Pattern Characteristics of High Pressure Boiling Water in Forced Convection, F. E. Tippets, April, 1962.

(9) GEAP-3148, Eccentric Rod Burnout at 1000 psi with Net Steam Generation, S. Levy, E. E. Polomik, C. L. Swan, A. W. McKinney (1959).